High order entropy stable and positivity-preserving discontinuous Galerkin method for the nonlocal electron heat transport model

Nuo Lei[1], Juan Cheng[2] and Chi-Wang Shu[3]

Abstract

The nonlocal electron heat transport model in laser heated plasmas plays a crucial role in inertial confinement fusion (ICF), and it is important to solve it numerically in an accurate and robust way. In this paper, we first develop an one-dimensional high-order entropy stable discontinuous Galerkin method for the nonlocal electron heat transport model. We further design our DG scheme to have the positivity-preserving property by using the scaling positivity-preserving limiter, which is shown, by a computer-aided proof, to have no extra time step constraint than that required by L^2 stability. Next, we extend our one-dimensional scheme to two-dimensions on rectangular meshes and tensor product polynomial spaces. Numerical examples are given to verify the high-order accuracy and positivity-preserving properties of our scheme. By comparing the local and nonlocal electron heat transport models, we also observe more physical phenomena such as the flux reduction and the preheat effect from the nonlocal model.

Keywords: Nonlocal electron heat transport; discontinuous Galerkin method; entropy stability; positivity-preserving; high order accuracy

[1]Graduate School, China Academy of Engineering Physics, Beijing 100088, China. E-mail: leinuo19@gscaep.ac.cn.

[2]Corresponding author. Laboratory of Computational Physics, Institute of Applied Physics and Computational Mathematics, Beijing 100088, China and HEDPS, Center for Applied Physics and Technology, and College of Engineering, Peking University, Beijing 100871, China. E-mail: cheng_juan@iapcm.ac.cn. Research is supported in part by NSFC grants 12031001 and 11871111, and CAEP Foundation No. CX20200026.

[3]Division of Applied Mathematics, Brown University, Providence, RI 02912. E-mail: chi-wang_shu@brown.edu. Research is supported in part by AFOSR grant FA9550-20-1-0055 and NSF grant DMS-2010107.

1 Introduction

In laser heated plasmas, the electron heat transport model which determines the energy distribution in plasmas plays a crucial role in inertial confinement fusion (ICF). The classical theory of thermal conductivity in plasma given by Spitzer and Harm [14, 25] is derived in the limit of small temperature gradients. However, when a steep temperature gradient appears in laser heated plasmas, the flux value obtained by the classical Spitzer-Harm model is several times higher than what is measured in the experiments, which is later interpreted as the nonlocal nature of the electron heat transport. The classical approach relates the heat flux with the temperature gradient and the heat conductivity in frequently collisional plasma, but it is not applicable in laser heated plasmas with weakly collisional plasma.

Although the nonlocal character of electron heat transport has been observed in many experiments, there is less development of adequate theory in this field. Based on the solution of the Fokker-Planck kinetic equation, Luciani et al. [22] proposed a nonlocal phenomenological formula in one dimension which could describe the effect of preheating, and this model has been adopted by many ICF simulation codes. Schurtz et al. [24] extended this formula to multidimensional cases and proposed a simpler equivalent transport equation which is easy to implement. The authors in [15] attempted to develop a nonlinear nonlocal transport model based on the self-similar solutions to the Fokker-Planck kinetic equation, but this model failed to describe the processes of nonlocal electron heat transport quantitatively [3, 4].

In this paper, we focus on the nonlocal electron heat transport model proposed by Schurtz et al. [24] which describes the diffusion term with desirable nonlocal damping properties,

$$\begin{cases} \partial_t u = -\nabla \cdot \vec{Q} \\ \vec{Q} = \vec{Q}_{SH} - \nabla \cdot (-\lambda \nabla \vec{Q}) \\ u(\mathbf{x}, 0) = u_0(\mathbf{x}) \\ (\mathbf{x}, t) \in \Omega \times [0, \infty) \end{cases} \tag{1.1}$$

where u is the electron temperature and $\vec{Q}$ is the heat flux. We denote $\vec{Q}_{SH}$ as the Spitzer-

Harm heat flux, that is

$$\vec{Q}_{SH} = -\kappa_{SH}\nabla u,$$

where κ_{SH} is the Spitzer heat conductivity [14, 25, 19],

$$\kappa_{SH} = \frac{Z + 0.24}{Z + 4.2}\frac{256\sqrt{2\pi}\varepsilon_0^2}{Ze^4\sqrt{m}\ln\Lambda}u^{\frac{5}{2}}.$$

Here ε_0 is the permittivity of the vacuum, Z is the average ionization of plasmas, e and m are the electron charge and mass, and $\ln\Lambda$ is the Coulomb logarithm, respectively. In this paper, we consider the more general type of the Spitzer-Harm heat flux $\vec{Q}_{SH}$ as

$$\vec{Q}_{SH} = -\nabla k(u)$$

where $k(u)$ is an increasing function of u, namely $k'(u) > 0$. The first equation in the nonlocal electron heat transport model (1.1) is a transport equation, with the global physical flux determined by the second stationary equation which is independent of time. Mathematical properties such as stability of similar equations are rarely mentioned in the literature.

There is also little discussion on how to numerically solve the model (1.1) accurately and robustly in the literature. In [24, 19], the authors applied second-order finite difference methods to find the approximation solutions for the nonlocal electron heat flux. This method is difficult to handle the solution with discontinuity or large gradient, in the meantime, it can not achieve high-order accuracy.

High-order discontinuous Galerkin methods coupled with the strong stability preserving Runge-Kutta (SSP-RK) time discretization [10, 9, 8, 11, 12] using discontinuous piecewise polynomial spaces are widely adopted for solving hyperbolic conservation laws accurately, due to their flexibility for complicated geometries even with hanging nodes and high parallel efficiency since cells only communicate with immediate neighbors. Besides the conservation laws, these methods have been extended to the local DG method [13], the ultra-weak DG method [7], etc., for dealing with diffusion terms and higher-order derivatives. Furthermore, DG methods have been designed to solve differential-algebraic systems such as the Vlasov-Poisson system in plasma physics of large ensembles of interaction [1, 2] and the drift-diffusion

model in semiconductor device simulations [20, 21]. For the model (1.1) that we are interested in, the first equation is a time-dependent transport equation and the second equation is a time-independent elliptic equation. Because of the many advantages of the DG methods mentioned above, we would like to design a high-order DG scheme for the nonlocal electron heat transport model (1.1).

Although the entropy inequality plays a crucial role in the well-posedness of the conservation laws, the classical DG method could satisfy the discrete square entropy inequality only for scalar equations and symmetric systems [18, 17]. Utilizing an entropy stable flux at the cell interfaces and the entropy conservative flux within cells, Chen and Shu [5, 6] proposed a framework of DG methods which could maintain high-order accuracy and conservation for the hyperbolic conservation laws and they could satisfy the entropy inequality for an arbitrary given convex entropy by using suitable numerical quadrature. Based on this framework, Sun et al. designed relevant high-order entropy stable DG methods for the nonlinear parabolic equations [26] and the cross-diffusion gradient flow system [27], which satisfy the discrete entropy inequality. Combined with the positivity-preserving limiter and the SSP-RK time discretization, their fully discretized scheme could keep positivity-preserving property and high-order accuracy. However, there is little discussion in the literature about the entropy inequality for the system composed of the time-dependent equation and the time-independent equation such as the electron heat transport model (1.1).

The temperature u in the nonlocal electron heat transport model (1.1) is physically non-negative, and negative temperature u makes the equation no longer well-posed. For example, in the Spitzer-Harm heat flux, we usually take $k(u) = C_{SH}u^{\frac{7}{2}}$ which requires $u \geq 0$. But we may get negative numerical solution by a numerical scheme particularly for the high-order scheme. Not only does negative numerical solution violates the physical properties, but it can also make the numerical scheme unstable or even fail the simulation when it is coupled with the fluid flow equations. Therefore, it is an important and challenging issue to design a high-order positivity-preserving scheme. Coupled with the explicit time discretization, a

series of positivity-preserving methods which satisfy a strict maximum principle or other bound-preserving properties have been developed for the conservation laws [31, 32, 33, 34], convection-diffusion equations [35], compressible Navier-Stokes equations [30], and other equations [29, 28], by using a positivity-preserving scaling limiter. Provable high-order accuracy and easiness for implementation make this positivity-preserving limiter widely adopted. By this method, the authors in [26, 27] have designed a positivity-preserving and entropy stable nodal DG scheme for the nonlinear parabolic equations and the cross-diffusion gradient flow system. This method requires the cell averages in the next time step remain non-negative if the solution at the previous time step is non-negative, only based on such assumption can we close the positivity-preserving loop.

All the above-mentioned positivity-preserving schemes are proposed for the explicit schemes. But the scheme we will design for the model (1.1) turns out to be an implicit type scheme because the second equation is independent of time. It is much more difficult to prove the cell averages are non-negative for an implicit high-order scheme if we know the numerical solution is non-negative at the previous time step. In fact, there is few discussion about the implicit high-order positivity-preserving scheme in the literature. Qin et al. [23] proposed a high-order positivity-preserving DG method with the implicit time discretization for the conservation laws.

In this paper, we would like to discuss some mathematical properties of the nonlocal electron heat transport model (1.1) first. Based on this, we develop a high-order entropy stable scheme with the DG space discretization and the SSP-RK time discretization in one dimension. Then we extend the scheme to two-dimensional rectangular meshes with tensor product polynomials. In order to preserve the positivity property of the temperature for our high-order implicit DG scheme, we would like to find a time step condition, by a computer-aided proof, that ensures the cell averages to be non-negative at the next time step if the solution at the current step is known to be non-negative. Then we can apply the scaling positivity-preserving limiter [31, 32, 33] to make sure the new solution is non-negative.

The outline of this paper is as follows. Section 2 and Section 3 describe the entropy stable high-order discontinuous Galerkin method for the one-dimensional and two-dimensional nonlocal electron heat transport models, respectively. After that, we will prove the semi-discrete scheme is conservative and satisfies discrete entropy inequality. Coupled with the SSP-RK time discretization and the positivity-preserving limiter, the fully discretized scheme is high-order accurate and preserves positivity of solutions under suitable time step restriction. Section 4 shows a series of numerical tests to examine the performance of the DG schemes for the one-dimensional and two-dimensional cases. Accuracy tests with or without the positivity-preserving limiter as well as non-oscillatory tests and positivity-preserving tests have been shown for the nonlocal model. Furthermore, we show several physical tests and observe significant differences in the effects of the local and nonlocal models. Finally, the conclusions and further comments are given in Section 5.

2 High-order entropy stable and positivity-preserving DG scheme for the one-dimensional nonlocal electron heat transport model

2.1 The stability property for the one-dimensional nonlocal electron heat transport model

We first consider the one-dimensional nonlocal electron heat transport model (1.1),

$$\begin{cases} \partial_t u = -\partial_x Q \\ Q = -\partial_x k(u) + \lambda \partial_{xx} Q \\ x \in \Omega \subset \mathbb{R}, \quad t > 0 \end{cases} \tag{2.1}$$

where we recall that $k'(u) > 0$. Define the convex function $U(u)$ such that $U'(u) = k(u)$, then the entropy functional

$$E = \int_\Omega U(u) dx$$

can be defined. For simplicity, we define Ω to be the connected compact domain with the periodic or compactly supported boundary condition. Zero-flux boundary condition can also

be used in Ω. After that we can show that the total entropy is non-increasing with respect to time,

$$\begin{aligned} \frac{dE}{dt} &= \int_\Omega k(u)u_t dx \\ &= \int_\Omega k(u)u_t dx + \int_\Omega \left[-k(u)_x Q + \lambda Q Q_{xx} - Q^2\right] dx \\ &= -\int_\Omega \left[Q_x k(u) + k(u)_x Q\right] dx - \int_\Omega \left(\lambda |Q_x|^2 + Q^2\right) dx \\ &= -\int_\Omega \left(\lambda |Q_x|^2 + Q^2\right) dx \leq 0. \end{aligned} \tag{2.2}$$

To be more specific, for the Spitzer-Harm local electron heat flux we have $\vec{Q}_{SH} = -C_{SH} u^{\frac{5}{2}} \nabla u$, $C_{SH} > 0$ [25, 14, 19], so the nonlinear term in our model (1.1) can be written as $k(u) = C_{SH} u^{\frac{7}{2}}$, therefore we can find the convex function $U = C_{SH} u^{\frac{9}{2}}$. Since the original equation satisfies such entropy inequality, and we would like to solve the nonlocal model robustly, so we hope our numerical scheme can inherit such properties. When the scheme satisfies similar discrete entropy inequality, it means that the scheme is entropy stable.

2.2 One-dimensional semi-discrete DG scheme for the nonlocal electron heat transport model

To design the discontinuous Galerkin method, by introducing the new variable G, we rewrite the original equations (2.1) as

$$\begin{cases} \partial_t u = -\partial_x Q \\ Q = -\lambda \partial_x G - \partial_x k(u) \\ G = -\partial_x Q \\ u(x,0) = u_0(x) \\ (x,t) \in \Omega \times [0,\infty) \end{cases} \tag{2.3}$$

where $\lambda \geq 0, k'(u) > 0$. We observe that there is no second order derivative terms in the system (2.3).

Suppose a regular partition of the domain $\Omega := \bigcup_{i=1}^{N} I_i$,

$$I_i = \left[x_{i-\frac{1}{2}}, x_{i+\frac{1}{2}}\right], \quad x_{\frac{1}{2}} < x_{\frac{3}{2}} <, \cdots, < x_{N+\frac{1}{2}}, \quad h_i = x_{i+\frac{1}{2}} - x_{i-\frac{1}{2}}, \quad h = \min_i h_i,$$

and the discrete discontinuous Galerkin space of polynomials of degree m

$$V^m = \{w(x) : w(x)|_{I_i} \in \mathcal{P}^m(I_i), 1 \leq i \leq N\}.$$

Here, $\mathcal{P}^m(I_i)$ is the space of polynomials of degree less than or equal to m on I_i.

Then we seek the numerical solution u_h, Q_h, G_h from V^m such that for any test function $\varphi, \phi_1, \phi_2 \in V^m$ and $1 \le i \le N$, we have

$$\begin{array}{rl} \int_{I_i} \partial_t u_h \varphi dx = & \int_{I_i} Q_h \partial_x \varphi dx - (\hat{Q}_h \varphi^-)_{i+\frac{1}{2}} + (\hat{Q}_h \varphi^+)_{i-\frac{1}{2}} \\ \int_{I_i} Q_h \phi_1 dx = & \lambda \int_{I_i} G_h \partial_x \phi_1 dx + \int_{I_i} k_h \partial_x \phi_1 dx \\ & -\lambda(\hat{G}_h \phi_1^-)_{i+\frac{1}{2}} + \lambda(\hat{G}_h \phi_1^+)_{i-\frac{1}{2}} - (\hat{k}_h \phi_1^-)_{i+\frac{1}{2}} + (\hat{k}_h \phi_1^+)_{i-\frac{1}{2}} \\ \int_{I_i} G_h \phi_2 dx = & \int_{I_i} Q_h \partial_x \phi_2 dx - (\hat{Q}_h \phi_2^-)_{i+\frac{1}{2}} + (\hat{Q}_h \phi_2^+)_{i-\frac{1}{2}} \end{array} \tag{2.4}$$

where we denote $k(u_h)$ as k_h, and $\hat{Q}_{h,i+\frac{1}{2}}, \hat{G}_{h,i+\frac{1}{2}}, \hat{k}_{h,i+\frac{1}{2}}$ are single-valued numerical fluxes at the cell interfaces of I_i and I_{i+1}, depending on the values of numerical solution from both sides $x^-_{i+\frac{1}{2}}, x^+_{i+\frac{1}{2}}$ etc. In this paper, we adopt the alternative numerical flux, i.e.

$$\hat{Q}_{h,i+\frac{1}{2}} = Q_h(x^-_{i+\frac{1}{2}}), \quad \hat{G}_{h,i+\frac{1}{2}} = G_h(x^+_{i+\frac{1}{2}}), \quad \hat{k}_{h,i+\frac{1}{2}} = k(u_h(x^+_{i+\frac{1}{2}})). \tag{2.5}$$

For simplicity, we omit the subscript h of the numerical solution u_h, Q_h, G_h in the following.

We apply the Gauss-Lobatto quadrature rule with $m+1$ quadrature points $\{x_i(\xi_r)\}_{r=0}^m$ on I_i,

$$x_i(\xi_r) := \frac{h_i}{2}\xi_r + \frac{1}{2}(x_{i-\frac{1}{2}} + x_{i+\frac{1}{2}}), \quad r = 0, 1, \cdots, m,$$

where $-1 = \xi_0 < \xi_1 <, \cdots, < \xi_m = 1$ and $\{\omega_r\}_{r=0}^m$ are the quadrature weights on $[-1, 1]$. Notice that its algebraic degree of accuracy is $2m-1$, so the Gauss-Lobatto quadrature, denoted by $\tilde{\int}_{I_i}$ below, is not exact for $\int_{I_i} \partial_t u \varphi dx, \int_{I_i} k \partial_x \phi_1 dx$, but is exact for $\int_{I_i} Q \partial_x \varphi dx$, $\int_{I_i} G \partial_x \phi_1 dx$, $\int_{I_i} Q \partial_x \phi_2 dx$.

Following the notations in [5], we define the Lagrangian nodal basis polynomials

$$L_j(\xi) = \prod_{\substack{l=0 \\ l \ne j}}^{m} \frac{\xi - \xi_l}{\xi_j - \xi_l},$$

and the function $u(x,t)$ on each cell I_i can be represented as

$$u(x,t) \mid_{I_i} = \sum_{r=0}^{m} u_r^i(t) L_r(\xi^i(x)), \quad x \in I_i,$$

here we use $u_r^i(t)$ to represent $u(x_i(\xi_r), t)$. The difference matrix D, the mass matrix M, the boundary matrix B and the stiffness matrix S are defined as

$$\begin{array}{rcl} D_{jl} & := & L_l'(\xi_j), \\ M & := & \mathrm{diag}\{\omega_0, \cdots, \omega_m\}, \\ B & := & \mathrm{diag}\{\tau_0, \cdots, \tau_m\} = \mathrm{diag}\{-1, 0, \cdots, 0, 1\}, \\ S_{jl} & := & \omega_j D_{jl}. \end{array} \tag{2.6}$$

In the meantime, we can prove the following summation-by-parts properties

Lemma 2.1. *According to the definition of the matrices (2.6), we have the following summation-by-parts properties which are the discrete analogues of the integration-by-parts properties,*

1) $S = MD, \quad MD + D^T M = S + S^T = B,$

2) $\sum_{l=0}^{m} D_{jl} = 0,\ 0 \le j \le m,$

3) $\sum_{l=0}^{m} S_{jl} = \sum_{l=0}^{m} \omega_j D_{jl} = 0,\ 0 \le j \le m,$

4) $\sum_{l=0}^{m} S_{lj} = \tau_j,\ 0 \le j \le m.$

The proof of Lemma 2.1 can be found in [5], so we omit it here. Then we use the quadrature rule $\tilde{\int}_{I_i}$ to substitute $\int_{I_i}$ in the weak form (2.4),

$$\begin{aligned}
\tilde{\int}_{I_i} \partial_t u \varphi dx &= \tilde{\int}_{I_i} Q \partial_x \varphi dx - (\hat{Q}\varphi^-)_{i+\frac{1}{2}} + (\hat{Q}\varphi^+)_{i-\frac{1}{2}} \\
\tilde{\int}_{I_i} Q \phi_1 dx &= \lambda \tilde{\int}_{I_i} G \partial_x \phi_1 dx + \tilde{\int}_{I_i} k \partial_x \phi_1 dx \\
&\quad -\lambda(\hat{G}\phi_1^-)_{i+\frac{1}{2}} + \lambda(\hat{G}\phi_1^+)_{i-\frac{1}{2}} - (\hat{k}\phi_1^-)_{i+\frac{1}{2}} + (\hat{k}\phi_1^+)_{i-\frac{1}{2}} \\
\tilde{\int}_{I_i} G \phi_2 dx &= \tilde{\int}_{I_i} Q \partial_x \phi_2 dx - (\hat{Q}\phi_2^-)_{i+\frac{1}{2}} + (\hat{Q}\phi_2^+)_{i-\frac{1}{2}}.
\end{aligned} \tag{2.7}$$

We denote the vectors $\vec{u}^i, \vec{Q}^i, \vec{G}^i, \vec{k}^i$ to be the values of u, Q, G, k at the Gauss-Lobatto quadrature points $\{x_i(\xi_r)\}_{r=0}^m$ within the cell I_i,

$$\begin{aligned}
\vec{u}^i &= [u(x_i(\xi_0)), \cdots, u(x_i(\xi_m))]^T, \quad \vec{Q}^i = [Q(x_i(\xi_0)), \cdots, Q(x_i(\xi_m))]^T, \\
\vec{G}^i &= [G(x_i(\xi_0)), \cdots, G(x_i(\xi_m))]^T, \quad \vec{k}^i = [k(x_i(\xi_0)), \cdots, k(x_i(\xi_m))]^T,
\end{aligned} \tag{2.8}$$

and define the numerical fluxes,

$$\begin{aligned}
\vec{Q}^{i,*} &= \left[\hat{Q}_{i-\frac{1}{2}}, 0, \cdots, 0, \hat{Q}_{i+\frac{1}{2}}\right]^T, \\
\vec{G}^{i,*} &= \left[\hat{G}_{i-\frac{1}{2}}, 0, \cdots, 0, \hat{G}_{i+\frac{1}{2}}\right]^T, \\
\vec{k}^{i,*} &= \left[\hat{k}_{i-\frac{1}{2}}, 0, \cdots, 0, \hat{k}_{i+\frac{1}{2}}\right]^T,
\end{aligned} \tag{2.9}$$

then the equations in (2.7) can be written as

$$\begin{aligned}
&\frac{h_i}{2} \left(\vec{\varphi}^i\right)^T M \frac{d\vec{u}^i}{dt} = (D\vec{\varphi}^i)^T M \vec{Q}^i - \left(\vec{\varphi}^i\right)^T B \vec{Q}^{i,*}, \\
&\frac{h_i}{2} \left(\vec{\phi}_1^i\right)^T M \vec{Q}^i = (D\vec{\phi}_1^i)^T M \left(\lambda \vec{G}^i + \vec{k}^i\right) - \left(\vec{\phi}_1^i\right)^T B \left(\lambda \vec{G}^{i,*} + \vec{k}^{i,*}\right), \\
&\frac{h_i}{2} \left(\vec{\phi}_2^i\right)^T M \vec{G}^i = (D\vec{\phi}_2^i)^T M \vec{Q}^i - \left(\vec{\phi}_2^i\right)^T B \vec{Q}^{i,*}.
\end{aligned}$$

Since the test functions φ, ϕ_1, ϕ_2 can be arbitrarily chosen from V^m, and applying the summation-by-parts properties given in Lemma 2.1, the above equations become

$$\begin{aligned}
\frac{h_i}{2}\frac{d\vec{u}^i}{dt} &= -D\vec{Q}^i - M^{-1}B\left(\vec{Q}^{i,*} - \vec{Q}^i\right) \\
\frac{h_i}{2}\vec{Q}^i &= -D\left(\lambda\vec{G}^i + \vec{k}^i\right) - M^{-1}B\left(\lambda\left(\vec{G}^{i,*} - \vec{G}^i\right) + \left(\vec{k}^{i,*} - \vec{k}^i\right)\right) \\
\frac{h_i}{2}\vec{G}^i &= -D\vec{Q}^i - M^{-1}B\left(\vec{Q}^{i,*} - \vec{Q}^i\right).
\end{aligned} \tag{2.10}$$

Now, we get the one-dimensional semi-discrete DG scheme (2.10). We will prove this DG scheme is conservative for the cell average $\bar{u}^i$ and entropy stable in the next subsection, after that, we will discuss how to design the DG scheme to have the positivity-preserving property under the Euler forward time discretization in Section 2.4.

2.3 Conservative and entropy stable properties of the one-dimensional semi-discrete DG scheme

In this subsection, we will prove our one-dimensional semi-discrete DG scheme (2.10) is conservative for the cell average $\bar{u}^i$ and satisfies the discrete entropy inequality.

Theorem 2.1. *Suppose $\vec{u}^i, \vec{Q}^i, \vec{G}^i, \vec{k}^i$ are obtained from the one-dimensional semi-discrete DG scheme (2.10). With the periodic or compactly supported boundary condition, the cell average $\bar{u}^i$ in the semi-discrete DG scheme (2.10) is conservative.*

Proof. For simplicity, we denote $u_r^i := u(x_i(\xi_r))$, $r = 0, 1, \cdots, m$, and denote the value of cell average to be $\bar{u}^i$ where $\bar{u}^i = \frac{1}{2}\sum_{r=0}^{m}\omega_r u_r^i$. We prove the conservation of temperature $\vec{u}$

on Ω,

$$\begin{aligned}
\frac{d\bar{u}^i h_i}{dt} &= \frac{h_i}{2}\sum_{r=0}^{m}\omega_r\frac{du_r^i}{dt} \\
&= -\sum_{r=0}^{m}\omega_r\sum_{l=0}^{m}D_{rl}Q_l^i - \sum_{r=0}^{m}\tau_r\left(Q_r^{i,*}-Q_r^i\right) \\
&= -\sum_{r=0}^{m}\tau_r\left(Q_r^{i,*}-Q_r^i\right) - \sum_{l=0}^{m}\sum_{r=0}^{m}S_{rl}Q_l^i \\
&= -\sum_{r=0}^{m}\tau_r\left(Q_r^{i,*}-Q_r^i\right) - \sum_{l=0}^{m}\tau_l Q_l^i \\
&= -\sum_{r=0}^{m}\tau_r Q_r^{i,*} \\
&= \hat{Q}_{i-\frac{1}{2}} - \hat{Q}_{i+\frac{1}{2}},
\end{aligned} \tag{2.11}$$

notice that we apply the periodic or compactly supported boundary condition, thus

$$\frac{d}{dt}\sum_{i=1}^{N}\bar{u}^i h_i = \sum_{i=1}^{N}\frac{d\bar{u}^i h_i}{dt} = \sum_{i=1}^{N}\left(\hat{Q}_{i-\frac{1}{2}} - \hat{Q}_{i+\frac{1}{2}}\right) = 0.$$

□

Generally speaking, the DG scheme for the conservation laws could not satisfy entropy conditions naturally, but in [5, 6], the authors modified the discrete derivative term in the DG scheme by the high-order, entropy conservative discrete flux to make them entropy stable. However, for some special systems such as the linear symmetric system and the p-system, the DG scheme itself could satisfy the entropy condition without the need of such modification. Luckily, our equation is somewhat similar to the p-system, so we can prove our scheme (2.10) is entropy stable without any modification on the original scheme.

Define the discrete entropy function

$$E := \tilde{\int_{\Omega}} U(u)dx = \sum_{i=1}^{N}\tilde{\int_{I_i}} U(u^i)dx.$$

Then the semi-discrete scheme (2.10) satisfies the following entropy inequality.

Theorem 2.2. *Suppose $\vec{u}^i, \vec{Q}^i, \vec{G}^i, \vec{k}^i$ are obtained from the one-dimensional semi-discrete DG scheme (2.10) and E is the associated discrete entropy function. Assume the boundary*

condition is periodic. Then, with the alternative numerical flux (2.5), we have

$$\frac{dE}{dt} = \sum_{i=1}^{N} \frac{dE^i}{dt} = \sum_{i=1}^{N} \tilde{\int_{I_i}} \frac{dU(u^i)}{dt} dx \leq 0.$$

Proof. Following the notations in the proof of Theorem 2.1, from the first equation of (2.10) we have

$$\begin{aligned} \frac{dE^i}{dt} &= \frac{h_i}{2} \vec{k}^{i,T} M \frac{d\vec{u}^i}{dt} \\ &= \vec{k}^{i,T} B \vec{Q}^i - \vec{k}^{i,T} B \vec{Q}^{i,*} - \vec{k}^{i,T} M D \vec{Q}^i \\ &= \vec{k}^{i,T} D^T M \vec{Q}^i - \vec{k}^{i,T} B \vec{Q}^{i,*} \end{aligned} \tag{2.12}$$

where the summation-by-parts property $B = MD + D^T M$ is adopted. Then, left multiply the second equation by $\vec{Q}^{i,T} M$ and left multiply the third equation by $\lambda \vec{G}^{i,T} M$ in the DG scheme (2.10),

$$\begin{aligned} \frac{h_i}{2} \vec{Q}^{i,T} M \vec{Q}^i =& \lambda \vec{Q}^{i,T} D^T M \vec{G}^i - \lambda \vec{Q}^{i,T} B \vec{G}^{i,*} + \vec{Q}^{i,T} D^T M \vec{k}^i - \vec{Q}^{i,T} B \vec{k}^{i,*}, \\ \lambda \frac{h_i}{2} \vec{G}^{i,T} M \vec{G}^i =& \lambda \vec{G}^{i,T} D^T M \vec{Q}^i - \lambda \vec{G}^{i,T} B \vec{Q}^{i,*}. \end{aligned} \tag{2.13}$$

Summing the above three equations, we have

$$\begin{aligned} & \frac{dE^i}{dt} + \frac{h_i}{2} \vec{Q}^{i,T} M \vec{Q}^i + \lambda \frac{h_i}{2} \vec{G}^{i,T} M \vec{G}^i \\ =& \vec{k}^{i,T} D^T M \vec{Q}^i - \vec{k}^{i,T} B \vec{Q}^{i,*} \\ & + \lambda \vec{Q}^{i,T} D^T M \vec{G}^i - \lambda \vec{Q}^{i,T} B \vec{G}^{i,*} + \vec{Q}^{i,T} D^T M \vec{k}^i - \vec{Q}^{i,T} B \vec{k}^{i,*} \\ & + \lambda \vec{G}^{i,T} D^T M \vec{Q}^i - \lambda \vec{G}^{i,T} B \vec{Q}^{i,*} \\ =& \lambda \left(\vec{Q}^{i,T} B \vec{G}^i - \vec{Q}^{i,T} B \vec{G}^{i,*} - \vec{G}^{i,T} B \vec{Q}^{i,*} \right) + \left(\vec{k}^{i,T} B \vec{Q}^i - \vec{k}^{i,T} B \vec{Q}^{i,*} - \vec{Q}^{i,T} B \vec{k}^{i,*} \right) \\ =& \lambda \left(Q^-_{i+\frac{1}{2}} G^-_{i+\frac{1}{2}} - Q^-_{i+\frac{1}{2}} \hat{G}_{i+\frac{1}{2}} - \hat{Q}_{i+\frac{1}{2}} G^-_{i+\frac{1}{2}} \right) - \lambda \left(Q^+_{i-\frac{1}{2}} G^+_{i-\frac{1}{2}} - Q^+_{i-\frac{1}{2}} \hat{G}_{i-\frac{1}{2}} - \hat{Q}_{i-\frac{1}{2}} G^+_{i-\frac{1}{2}} \right) \\ & + \left(Q^-_{i+\frac{1}{2}} k^-_{i+\frac{1}{2}} - Q^-_{i+\frac{1}{2}} \hat{k}_{i+\frac{1}{2}} - \hat{Q}_{i+\frac{1}{2}} k^-_{i+\frac{1}{2}} \right) - \left(Q^+_{i-\frac{1}{2}} k^+_{i-\frac{1}{2}} - Q^+_{i-\frac{1}{2}} \hat{k}_{i-\frac{1}{2}} - \hat{Q}_{i-\frac{1}{2}} k^+_{i-\frac{1}{2}} \right), \end{aligned} \tag{2.14}$$

where there are only boundary terms at the right hand side. If we take the alternative numerical flux (2.5) on the common interface of the cells I_i and I_{i+1}, the boundary term

$\vec{Q}^{i,T}B\vec{G}^i - \vec{Q}^{i,T}B\vec{G}^{i,*} - \vec{G}^{i,T}B\vec{Q}^{i,*}$ becomes

$$\begin{aligned}
&\left(Q^-_{i+\frac{1}{2}}G^-_{i+\frac{1}{2}} - Q^-_{i+\frac{1}{2}}\hat{G}_{i+\frac{1}{2}} - \hat{Q}_{i+\frac{1}{2}}G^-_{i+\frac{1}{2}}\right) - \left(Q^+_{i+\frac{1}{2}}G^+_{i+\frac{1}{2}} - Q^+_{i+\frac{1}{2}}\hat{G}_{i+\frac{1}{2}} - \hat{Q}_{i+\frac{1}{2}}G^+_{i+\frac{1}{2}}\right)\\
=&\left(Q^-_{i+\frac{1}{2}}G^-_{i+\frac{1}{2}} - Q^-_{i+\frac{1}{2}}G^+_{i+\frac{1}{2}} - Q^-_{i+\frac{1}{2}}G^-_{i+\frac{1}{2}}\right) - \left(Q^+_{i+\frac{1}{2}}G^+_{i+\frac{1}{2}} - Q^+_{i+\frac{1}{2}}G^+_{i+\frac{1}{2}} - Q^-_{i+\frac{1}{2}}G^+_{i+\frac{1}{2}}\right)\\
=&0,
\end{aligned} \tag{2.15}$$

and the boundary term $\vec{k}^{i,T}B\vec{Q}^i - \vec{k}^{i,T}B\vec{Q}^{i,*} - \vec{Q}^{i,T}B\vec{k}^{i,*}$ becomes

$$\begin{aligned}
&\left(Q^-_{i+\frac{1}{2}}k^-_{i+\frac{1}{2}} - Q^-_{i+\frac{1}{2}}\hat{k}_{i+\frac{1}{2}} - \hat{Q}_{i+\frac{1}{2}}k^-_{i+\frac{1}{2}}\right) - \left(Q^+_{i+\frac{1}{2}}k^+_{i+\frac{1}{2}} - Q^+_{i+\frac{1}{2}}\hat{k}_{i+\frac{1}{2}} - \hat{Q}_{i+\frac{1}{2}}k^+_{i+\frac{1}{2}}\right)\\
=&\left(Q^-_{i+\frac{1}{2}}k^-_{i+\frac{1}{2}} - Q^-_{i+\frac{1}{2}}k^+_{i+\frac{1}{2}} - Q^-_{i+\frac{1}{2}}k^-_{i+\frac{1}{2}}\right) - \left(Q^+_{i+\frac{1}{2}}k^+_{i+\frac{1}{2}} - Q^+_{i+\frac{1}{2}}k^+_{i+\frac{1}{2}} - Q^-_{i+\frac{1}{2}}k^+_{i+\frac{1}{2}}\right)\\
=&0.
\end{aligned} \tag{2.16}$$

After summing over the index i and using the periodic property, we obtain

$$\begin{aligned}
\frac{dE}{dt} =& \sum_{i=1}^{N}\frac{dE^i}{dt}\\
=& -\sum_{i=1}^{N}\frac{h_i}{2}\left(\vec{Q}^{i,T}M\vec{Q}^i + \lambda\vec{G}^{i,T}M\vec{G}^i\right) \le 0,
\end{aligned} \tag{2.17}$$

due to the non-negativity of λ. □

Remark 2.1. *Besides the alternative numerical flux (2.5), we can also choose the combination of the Lax-Friedrichs numerical flux for $\hat{Q}$ and the central numerical flux for $\hat{G}, \hat{k}$, i.e.*

$$\begin{aligned}
&\hat{Q}_{i+\frac{1}{2}} = \frac{Q(x^+_{i+\frac{1}{2}}) + Q(x^-_{i+\frac{1}{2}})}{2} - \alpha\left(G(x^+_{i+\frac{1}{2}}) - G(x^-_{i+\frac{1}{2}})\right) - \frac{\alpha}{\lambda}\left(k(x^+_{i+\frac{1}{2}}) - k(x^-_{i+\frac{1}{2}})\right),\\
&\qquad \textit{where} \quad \alpha \ge 0,\ \lambda \ne 0,\\
&\hat{G}_{i+\frac{1}{2}} = \frac{G(x^+_{i+\frac{1}{2}}) + G(x^-_{i+\frac{1}{2}})}{2}, \quad \hat{k}_{i+\frac{1}{2}} = \frac{k(x^+_{i+\frac{1}{2}}) + k(x^-_{i+\frac{1}{2}})}{2}.
\end{aligned} \tag{2.18}$$

Then, the two boundary terms of (2.14) become

$$\begin{aligned}
&\left(Q^-_{i+\frac{1}{2}}G^-_{i+\frac{1}{2}} - Q^-_{i+\frac{1}{2}}\hat{G}_{i+\frac{1}{2}} - \hat{Q}_{i+\frac{1}{2}}G^-_{i+\frac{1}{2}}\right) - \left(Q^+_{i+\frac{1}{2}}G^+_{i+\frac{1}{2}} - Q^+_{i+\frac{1}{2}}\hat{G}_{i+\frac{1}{2}} - \hat{Q}_{i+\frac{1}{2}}G^+_{i+\frac{1}{2}}\right)\\
=& -\alpha_{i+\frac{1}{2}}\left[G_{i+\frac{1}{2}}\right]^2 - \frac{\alpha_{i+\frac{1}{2}}}{\lambda}\left[k_{i+\frac{1}{2}}\right]\left[G_{i+\frac{1}{2}}\right],
\end{aligned} \tag{2.19}$$

and

$$\begin{aligned}
&\left(Q^-_{i+\frac{1}{2}}k^-_{i+\frac{1}{2}} - Q^-_{i+\frac{1}{2}}\hat{k}_{i+\frac{1}{2}} - \hat{Q}_{i+\frac{1}{2}}k^-_{i+\frac{1}{2}}\right) - \left(Q^+_{i+\frac{1}{2}}k^+_{i+\frac{1}{2}} - Q^+_{i+\frac{1}{2}}\hat{k}_{i+\frac{1}{2}} - \hat{Q}_{i+\frac{1}{2}}k^+_{i+\frac{1}{2}}\right)\\
=& -\frac{\alpha_{i+\frac{1}{2}}}{\lambda}\left[k_{i+\frac{1}{2}}\right]^2 - \alpha_{i+\frac{1}{2}}\left[k_{i+\frac{1}{2}}\right]\left[G_{i+\frac{1}{2}}\right],
\end{aligned} \tag{2.20}$$

where we introduce the average form and the jump form

$$[G] := G^+ - G^-, \quad \{G\} := \frac{1}{2}(G^- + G^+).$$

After summing over the index i and using the periodic property, we can obtain the discrete entropy inequality

$$\begin{aligned} \frac{dE}{dt} =& \sum_{i=1}^{N} \frac{dE^i}{dt} \\ =& -\sum_{i=1}^{N} \frac{h_i}{2} \left(\vec{Q}^{i,T} M \vec{Q}^i + \lambda \vec{G}^{i,T} M \vec{G}^i \right) - \sum_{i=1}^{N} \frac{\alpha_{i+\frac{1}{2}}}{\lambda} \left(\lambda [G_{i+\frac{1}{2}}] + [k_{i+\frac{1}{2}}] \right)^2 \\ \leq& 0. \end{aligned} \tag{2.21}$$

2.4 The positivity-preserving property for the one-dimensional fully discretized DG scheme

We consider the Euler forward time discretization method for the one-dimensional semi-discrete DG scheme (2.10) with $\lambda > 0$,

$$\begin{aligned} \frac{h_i}{2} \frac{\vec{u}^{i,\mathrm{pre}} - \vec{u}^{i,n}}{\tau} &= -D\vec{Q}^i - M^{-1} B(\vec{Q}^{i,*} - \vec{Q}^i) \\ \frac{h_i}{2} \vec{Q}^i &= -D(\lambda \vec{G}^i + \vec{k}^i) - M^{-1} B(\lambda(\vec{G}^{i,*} - \vec{G}^i) + (\vec{k}^{i,*} - \vec{k}^i)) \\ \frac{h_i}{2} \vec{G}^i &= -D\vec{Q}^i - M^{-1} B(\vec{Q}^{i,*} - \vec{Q}^i), \end{aligned} \tag{2.22}$$

where n represents n-th time step and the superscript *pre* represents the solution obtained from the Euler forward method before applying any limiter.

Lemma 2.2. *Consider the linear function $k(u) = u$, the uniform mesh $h := h_i$, $\forall i$ and the periodic boundary condition. The one-dimensional fully discretized DG scheme (2.22) is stable under the time step condition*

$$\tau \leq \max\{\lambda, c_m h^2\}, \tag{2.23}$$

where c_m is a constant which depends only on the polynomial degree m of the DG space, $c_m \in (0.01, 1)$ which is obtained by the Fourier analysis numerically.

We adopt the Fourier analysis [23] to prove this lemma and verify the stability of the DG scheme with different τ and λ numerically. In Figure 2.1, we show the stability region

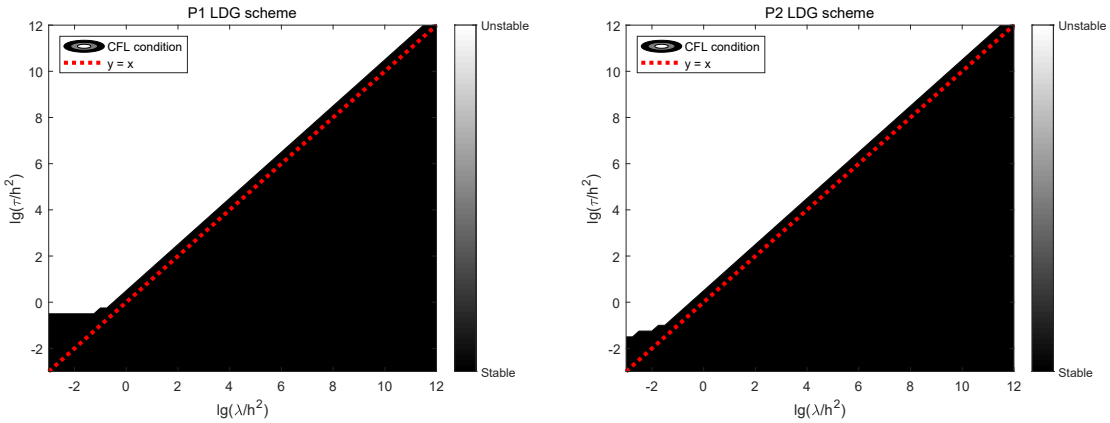

Figure 2.1: The stability region corresponding to the maximum time step τ and the nonlocal parameter λ for the one-dimensional DG scheme. The DG scheme is stable when λ, τ are in the black region. Left: the one-dimensional DG scheme with $m = 1$; Right: the one-dimensional DG scheme with $m = 2$.

corresponding to the maximum time step τ and the nonlocal parameter λ for the one-dimensional DG scheme. One can see the DG scheme for $m = 1, 2$ are stable as long as $\tau \leq \lambda$. For $m \geq 3$, we have done the same analysis and have obtained the same results. This stability condition is also valid for the higher order Runge-Kutta time discretizations.

This time step condition (2.23) implies that the explicit scheme for the model (2.1) is "unconditionally" stable, in the sense that the time step needs only to be upper bounded by a constant $\tau \leq \lambda$, which is independent of the mesh size h. This appears to be surprising for an explicit scheme, however this is reasonable as the solution operator is zeroth order (a bounded operator) for $\lambda > 0$ according to the analysis in Appendix A. When λ is very small and the mesh size h is relatively large, the maximum in (2.23) should take the value of the time step restriction $\tau \leq c_m h^2$. This will also be the time step restriction for the local case with $\lambda = 0$. Based on this, we will further develop an one-dimensional positivity-preserving fully discretized DG scheme.

In the nonlocal electron heat transport model, the temperature u is physically non-negative, thus the results of the DG scheme should keep this property. A general framework to achieve bound-preserving property without affecting the original high order accuracy for the DG methods has been proposed in [31, 32, 33], and we will design our scheme to have

the positivity-preserving property by using this general framework.

The positivity-preserving procedure developed in [31, 32, 33] consists of the following two steps:

1. Consider the Euler forward time discretization, we need to make sure the cell averages of the solution produced by the DG scheme (2.22) are positive, provided the solution is positive at the current time step, which means that the solution values at all the quadrature points are positive.

2. Once the cell averages at the next time step are positive and high order accurate, and the DG solution at the next time step is high order accurate but may not be positive, then the scaling positivity-preserving limiter in [31, 32, 33] can be used to enforce the positivity of the solution at all of the quadrature points, and it is proved in [31, 32, 33] that this scaling positivity-preserving limiter maintains the original high order accuracy.

The second step is independent of the equation being used and the numerical method being adopted, while the first step needs to be proved for different equations and schemes individually. We will prove the first step for our method below.

We assume the provided solution $\vec{u}^{i,n}$, $\forall i = 1, \cdots, N$ are positive at all quadrature points and we would like to prove that the new cell averages $\bar{u}^{i,\text{pre}}$, $\forall i = 1, \cdots, N$ are positive. Since our scheme (2.22) are of an implicit type (global dependency) about the heat flux $\vec{Q}^i$, which is different from the explicit scheme discussed in [31, 32, 33], the approach in these references cannot be applied. Referring to [23] where the authors designed an implicit high-order positivity-preserving DG scheme for the conservation laws, we also try to design a positivity-preserving DG scheme for the nonlocal electron heat transport model (2.1) under a suitable time step condition.

Theorem 2.3. *Suppose $k(u)$ is a function with continuous derivative, the mesh is uniform $h := h_i$, $\forall i$ and the boundary condition is periodic. Suppose the mesh size h is small enough,*

that is $h < \sqrt{\frac{\lambda}{d_m}}$, *where* d_m *is a constant which depends only on the polynomial degree* m *of the DG space and* $d_m \in [0.01, 0.1]$ *according to the Fourier analysis numerically. Assume* $u^n(x_i(\xi_r)) \geq 0$ *at all quadrature points, then the solution of the one-dimensional fully discretized DG scheme* (2.22) *with the alternative numerical flux* (2.5) *satisfies* $\bar{u}^{i,pre} \geq 0$ *under the time step condition*

$$\max_{1\leq i\leq N, 0\leq r\leq m} k'(u^n(x_i(\xi_r)))\tau \leq \lambda, \tag{2.24}$$

where $\max_{1\leq i\leq N,0\leq r\leq m} k'(u^n(x_i(\xi_r)))$ *means the maximum value of* $k'(u)$ *at all of the quadrature points* $x_i(\xi_r)$.

Proof. Since the mesh is uniform and the boundary condition is periodic with the alternative numerical flux (2.5), the one-dimensional DG scheme (2.22) can be written as

$$\begin{array}{rcl} \frac{h}{2}M\frac{\vec{u}^{i,\mathrm{pre}}-\vec{u}^{i,n}}{\tau} & = & \mathcal{A}_u\vec{Q}^i + \mathcal{B}_u\vec{Q}^{i-1} \\ \frac{h}{2}M\vec{Q}^i & = & \mathcal{A}_d(\vec{k}^i + \lambda\vec{G}^i) + \mathcal{B}_d(\vec{k}^{i+1} + \lambda\vec{G}^{i+1}) \\ \frac{h}{2}M\vec{G}^i & = & \mathcal{A}_u\vec{Q}^i + \mathcal{B}_u\vec{Q}^{i-1}, \end{array} \tag{2.25}$$

where

$$\mathcal{A}_u = D^TM + \begin{pmatrix} 0 & & \\ & \ddots & \\ & & -1 \end{pmatrix}, \qquad \mathcal{B}_u = \begin{pmatrix} 0 & & 1 \\ & \ddots & \\ & & 0 \end{pmatrix},$$

$$\mathcal{A}_d = D^TM + \begin{pmatrix} 1 & & \\ & \ddots & \\ & & 0 \end{pmatrix}, \qquad \mathcal{B}_d = \begin{pmatrix} 0 & & \\ & \ddots & \\ -1 & & 0 \end{pmatrix}.$$

In the meantime, if we define long vectors of length $(m+1)N$

$$\begin{array}{rclrcl} \boldsymbol{u} & := & [\vec{u}^1, \cdots, \vec{u}^N]^T, & \boldsymbol{Q} & := & [\vec{Q}^1, \cdots, \vec{Q}^N]^T, \\ \boldsymbol{G} & := & [\vec{G}^1, \cdots, \vec{G}^N]^T, & \boldsymbol{k} & := & [\vec{k}^1, \cdots, \vec{k}^N]^T, \end{array} \tag{2.26}$$

then the DG scheme (2.25) can be written as

$$\begin{array}{rcl} \frac{h}{2}\mathcal{M}\frac{\boldsymbol{u}^{\mathrm{pre}}-\boldsymbol{u}^n}{\tau} & = & \mathcal{D}_u\boldsymbol{Q} \\ \frac{h}{2}\mathcal{M}\boldsymbol{Q} & = & \mathcal{D}_d(\boldsymbol{k} + \lambda\boldsymbol{G}) \\ \frac{h}{2}\mathcal{M}\boldsymbol{G} & = & \mathcal{D}_u\boldsymbol{Q}, \end{array} \tag{2.27}$$

where $\mathcal{M}, \mathcal{D}_u, \mathcal{D}_d$ are $(m+1)N \times (m+1)N$ matrices

$$\mathcal{M} = \begin{pmatrix} M & \mathcal{O} & \cdots & \mathcal{O} \\ \mathcal{O} & M & \ddots & \vdots \\ \vdots & \ddots & \ddots & \mathcal{O} \\ \mathcal{O} & \cdots & \mathcal{O} & M \end{pmatrix}, \ \mathcal{D}_u = \begin{pmatrix} \mathcal{A}_u & \mathcal{O} & \cdots & \mathcal{B}_u \\ \mathcal{B}_u & \mathcal{A}_u & \ddots & \vdots \\ \vdots & \ddots & \ddots & \mathcal{O} \\ \mathcal{O} & \cdots & \mathcal{B}_u & \mathcal{A}_u \end{pmatrix}, \ \mathcal{D}_d = \begin{pmatrix} \mathcal{A}_d & \mathcal{B}_d & \cdots & \mathcal{O} \\ \mathcal{O} & \mathcal{A}_d & \ddots & \vdots \\ \vdots & \ddots & \ddots & \mathcal{B}_d \\ \mathcal{B}_d & \cdots & \mathcal{O} & \mathcal{A}_d \end{pmatrix}.$$

First we consider the linear function $k(u) = u$, then we have

$$\begin{aligned}\boldsymbol{u}^{\text{pre}} =& \boldsymbol{u} + \frac{2\tau}{h}\mathcal{M}^{-1}\mathcal{D}_u\boldsymbol{Q} \\ =& \boldsymbol{u} + \frac{4\tau}{h^2}\mathcal{M}^{-1}\mathcal{D}_u\left(\mathcal{I} - \frac{4\lambda}{h^2}\mathcal{M}^{-1}\mathcal{D}_d\mathcal{M}^{-1}\mathcal{D}_u\right)^{-1}\mathcal{M}^{-1}\mathcal{D}_d\boldsymbol{u} \\ =& \left[\mathcal{I} + \frac{4\tau}{h^2}\mathcal{M}^{-1}\mathcal{D}_u\left(\mathcal{I} - \frac{4\lambda}{h^2}\mathcal{M}^{-1}\mathcal{D}_d\mathcal{M}^{-1}\mathcal{D}_u\right)^{-1}\mathcal{M}^{-1}\mathcal{D}_d\right]\boldsymbol{u},\end{aligned} \tag{2.28}$$

where $\mathcal{I}$ is $(m+1)N \times (m+1)N$ identity matrix. Since the cell averages can be described as

$$\bar{u}^i = \frac{1}{2}\sum_{r=0}^{m}\omega_r u(x_i(\xi_r)) = \frac{\vec{\omega}^T}{2}\vec{u}^i, \quad \vec{\omega} = [\omega_0, \cdots, \omega_m]^T,$$

by the equation (2.28), the cell-average vector $\bar{\boldsymbol{u}}^{\text{pre}} := [\bar{u}^{1,\text{pre}}, \cdots, \bar{u}^{N,\text{pre}}]^T$ of length N and $N \times (m+1)N$ matrix Ave can be written as

$$\text{Ave} := \begin{pmatrix} \frac{\vec{\omega}}{2} & & \\ & \ddots & \\ & & \frac{\vec{\omega}}{2} \end{pmatrix}\left[\mathcal{I} + \frac{4\tau}{h^2}\mathcal{M}^{-1}\mathcal{D}_u\left(\mathcal{I} - \frac{4\lambda}{h^2}\mathcal{M}^{-1}\mathcal{D}_d\mathcal{M}^{-1}\mathcal{D}_u\right)^{-1}\mathcal{M}^{-1}\mathcal{D}_d\right],$$

so we have $\bar{\boldsymbol{u}}^{\text{pre}} = \text{Ave}\boldsymbol{u}$. Then, we need to check every element in Ave is non-negative. As it is difficult to demonstrate it analytically since its form is too complicated, we will check it numerically. In practice, since the matrices $\mathcal{M}, \mathcal{D}_u, \mathcal{D}_d$ are known, if we give $\frac{\lambda}{h^2}, \frac{\tau}{h^2}$ specific values, we can calculate the matrix Ave and then check every element in Ave is non-negative. In our numerical experiments, $\frac{\lambda}{h^2}, \frac{\tau}{h^2}$ are taken from $[10^{-4}, 10^{12}]$.

We show the numerical results for the DG scheme with $m = 1, 2$ and $k(u) = u$, in Figure 2.2. For different values of $\frac{\lambda}{h^2}, \frac{\tau}{h^2}$, if there is no negative value in the matrix Ave, that means the cell averages can preserve non-negativity with non-negative input values $u^n(x_i(\xi_r))$, we mark it by the black color; otherwise, we mark it by the white color.

For $m = 2$, we can see that from the bottom left of the right subfigure of Figure 2.2, when the mesh size h is small enough, more precisely when $h \leq \sqrt{\frac{\lambda}{d_m}}$, and when the time step satisfies $\tau \leq \lambda$ since $k'(u) = 1$, the cell averages $\bar{u}^{i,\text{pre}}$ can preserve non-negativity. This time step condition coincides with that for the stability property of our DG scheme which is given in Lemma 2.2. For the one-dimensional DG scheme with $m > 2$, we have done the same analysis and have obtained the same result as that for $m = 2$.

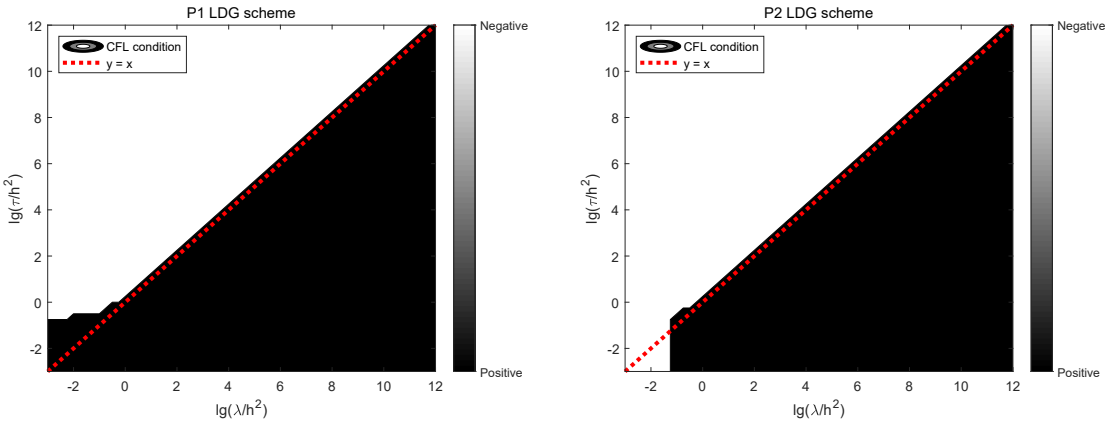

Figure 2.2: The positivity-preserving region corresponding to the maximum time step τ and the nonlocal parameter λ for the one-dimensional DG scheme with the linear function $k(u) = u$. The cell averages $\bar{\boldsymbol{u}}^{\text{pre}}$ can preserve positivity when λ, τ are in the black region. Left: the one-dimensional DG scheme with $m = 1$; Right: the one-dimensional DG scheme with $m = 2$.

For $m = 1$, from the left subfigure of Figure 2.2, we can see that for any h and λ, if the time step condition satisfies $\tau \leq \lambda$ then we can design a positivity-preserving DG scheme for the model (2.1). In general, for $m \geq 2$ and $\lambda > 0$, the mesh size restriction $h < \sqrt{\frac{\lambda}{d_m}}$ is very mild. While for the local case $\lambda = 0$ and $m \geq 2$, we can always find counterexamples under certain initial condition where negative values of the cell average appear at the next time step. Then we can not design a positivity-preserving DG scheme for the model (2.1).

We can generalize the above proof for the linear function $k(u) = u$ to the more general linear function $k(u) = \mu u$ where $\mu \geq 0$ is a constant and $\boldsymbol{u}^{\text{pre}}$ can be written as

$$\boldsymbol{u}^{\text{pre}} = \left[\mathcal{I} + \mu\frac{4\tau}{h^2}\mathcal{M}^{-1}\mathcal{D}_u\left(\mathcal{I} - \frac{4\lambda}{h^2}\mathcal{M}^{-1}\mathcal{D}_d\mathcal{M}^{-1}\mathcal{D}_u\right)^{-1}\mathcal{M}^{-1}\mathcal{D}_d\right]\boldsymbol{u}.$$

Then, the time step condition for $\bar{\boldsymbol{u}}^{\text{pre}} \geq 0$ is $\mu\tau \leq \lambda$.

For the nonlinear case, we consider it as a quasilinear function $k(u) = k'(u)u$ and then $\boldsymbol{u}^{\text{pre}}$ can be written as

$$\boldsymbol{u}^{\text{pre}} = \left[\mathcal{I} + k'(\boldsymbol{u})\frac{4\tau}{h^2}\mathcal{M}^{-1}\mathcal{D}_u\left(\mathcal{I} - \frac{4\lambda}{h^2}\mathcal{M}^{-1}\mathcal{D}_d\mathcal{M}^{-1}\mathcal{D}_u\right)^{-1}\mathcal{M}^{-1}\mathcal{D}_d\right]\boldsymbol{u}.$$

Then, the time step condition for $\bar{\boldsymbol{u}}^{\text{pre}} \geq 0$ is

$$\max_{1\leq i\leq N, 0\leq r\leq m} k'(u^n(x_i(\xi_r)))\tau \leq \lambda.$$

□

As a result, under the time step condition (2.24) and when the mesh size h is suitably small, the cell averages obtained by the DG scheme (2.22) with the Euler forward time discretization are non-negative, provided that the solution values at all quadrature points are non-negative at the current time step. Based on the non-negative cell average values, we adopt the following scaling positivity-preserving limiter proposed by Zhang and Shu [31, 32, 33] to ensure the non-negativity of the values at all the quadrature points at the next time step,

$$u^{n+1}(x_i(\xi_r)) = \bar{u}^{i,\text{pre}} + \theta_i \left(u^{\text{pre}}(x_i(\xi_r)) - \bar{u}^{i,\text{pre}}\right), \quad 0 \le r \le m, \tag{2.29}$$

where $\theta_i = \min\left\{1, \frac{\bar{u}^{i,\text{pre}}-\varepsilon}{\bar{u}^{i,\text{pre}}-m_i}\right\}$, $m_i = \min\limits_{0\le r\le m}\{u^{\text{pre}}(x_i(\xi_r))\}$ and usually we take $\varepsilon = 10^{-16}$. Then the values at the quadrature points $u^{n+1}(x_i(\xi_r))$ are all non-negative and the loop is closed. Beyond this, the scaling positivity-preserving limiter will not destroy the original accuracy which has been proved in [31, 32, 33] and we will show several numerical tests in Section 4.1.2 and Section 4.2.2 to verify this property.

Next, we will prove that the positivity-preserving limiter does not destroy the entropy stability if we assume the one-dimensional fully discretized original DG scheme with the Euler forward time discretization (2.22) is entropy stable.

Theorem 2.4. *If we change the solution of* (2.22) $u(x_i(\xi_r))$, $1 \le i \le N$, $0 \le r \le m$, *to* $u^{new}(x_i(\xi_r))$ *as*

$$u^{new}(x_i(\xi_r)) = \bar{u}^i + \theta_r^i(u(x_i(\xi_r)) - \bar{u}^i), \quad 0 \le \theta_r^i \le 1$$

then for any convex entropy function U, the discrete entropy does not increase, that is,

$$E^{new} = \frac{1}{2}\sum_{r=0}^{m} \omega_r U(u^{new}(x_i(\xi_r))) \le \frac{1}{2}\sum_{r=0}^{m} \omega_r U(u(x_i(\xi_r))) = E,$$

where $\frac{1}{2}\sum_{r=0}^{m}\omega_r = 1$. *That means the scaling positivity-preserving limiter* (2.29) *does not increase the discrete entropy.*

Proof. First, it is easy to prove that the average $\bar{u}^i$ does not change after the positivity-preserving limiter is used.

$$\frac{1}{2}\sum_{r=0}^{m}\omega_r u(x_i(\xi_r)) = \bar{u}^i = \frac{1}{2}\sum_{r=0}^{m}\omega_r u^{\text{new}}(x_i(\xi_r)).$$

Then we have

$$\begin{aligned}
&\frac{1}{2}\sum_{r=0}^{m}\omega_r u(x_i(\xi_r)) = \frac{1}{2}\sum_{r=0}^{m}\omega_r\left[(1-\theta_r^i)\bar{u}^i + \theta_r^i u(x_i(\xi_r))\right] \\
\Rightarrow &\sum_{r=0}^{m}\omega_r(1-\theta_r^i)u(x_i(\xi_r)) = \left(\sum_{r=0}^{m}\omega_r(1-\theta_r^i)\right)\bar{u}^i,
\end{aligned}$$

and

$$\begin{aligned}
&\bar{u}^i = \frac{1}{2}\sum_{r=0}^{m}\omega_r\bar{u}^i = \frac{1}{2}\sum_{r=0}^{m}\omega_r u^{\text{new}}(x_i(\xi_r)) \\
\Rightarrow &\frac{1}{2}\sum_{r=0}^{m}\omega_r\bar{u}^i = \frac{1}{2}\sum_{r=0}^{m}\omega_r\left[(1-\theta_r^i)\bar{u}^i + \theta_r^i u(x_i(\xi_r))\right] \\
\Rightarrow &\sum_{r=0}^{m}\omega_r\theta_r^i u(x_i(\xi_r)) = \left(\sum_{r=0}^{m}\omega_r\theta_r^i\right)\bar{u}^i.
\end{aligned}$$

By the convexity of the function U

$$U(u^{\text{new}}(x_i(\xi_r))) \le \theta_r^i U(u(x_i(\xi_r))) + (1-\theta_r^i)U(\bar{u}^i),$$

since

$$\begin{aligned}
\sum_{r=0}^{m}\frac{\omega_r}{2}U(\bar{u}^i) = U(\bar{u}^i) &= U\left(\sum_{r=0}^{m}\frac{\omega_r}{2}\bar{u}^i\right) \\
&= U\left(\sum_{r=0}^{m}\frac{\omega_r}{2}\left[(1-\theta_r^i)\bar{u}^i + \theta_r^i\bar{u}^i\right]\right) \\
&= U\left(\sum_{r=0}^{m}\frac{\omega_r}{2}\left[(1-\theta_r^i)u(x_i(\xi_r)) + \theta_r^i\bar{u}^i\right]\right) \\
&\le \sum_{r=0}^{m}\frac{\omega_r}{2}U\left((1-\theta_r^i)u(x_i(\xi_r)) + \theta_r^i\bar{u}^i\right) \\
&\le \sum_{r=0}^{m}\frac{\omega_r}{2}(1-\theta_r^i)U(u(x_i(\xi_r))) + \sum_{r=0}^{m}\frac{\omega_r}{2}\theta_r^i U(\bar{u}^i)
\end{aligned}$$

so we have

$$\frac{1}{2}\left(\sum_{r=0}^{m}\omega_r(1-\theta_r^i)\right)U(\bar{u}^i) \le \frac{1}{2}\sum_{r=0}^{m}\omega_r(1-\theta_r^i)U(u(x_i(\xi_r))).$$

Hence

$$\begin{aligned}\frac{1}{2}\sum_{r=0}^{m}\omega_r U(u^{\text{new}}(x_i(\xi_r))) &\le \frac{1}{2}\sum_{r=0}^{m}\omega_r\left(\theta_r^i U(u(x_i(\xi_r))) + (1-\theta_r^i)U(\bar{u}^i)\right)\\ &\le \frac{1}{2}\sum_{r=0}^{m}\omega_r\left(\theta_r^i U(u(x_i(\xi_r))) + (1-\theta_r^i)U(u(x_i(\xi_r)))\right)\\ &= \frac{1}{2}\sum_{r=0}^{m}\omega_r U(u(x_i(\xi_r))).\end{aligned} \tag{2.30}$$

This means $E^{new} \le E$.

We will show the decay of discrete entropy in the numerical example. □

Assume that we have already known the solution vector $\boldsymbol{u}$ at the n-th time step. Denote $\boldsymbol{F}(\boldsymbol{u})$ as the spatial operator in the DG scheme (2.10), i.e.,

$$\frac{d\boldsymbol{u}}{dt} = \boldsymbol{F}(\boldsymbol{u})$$

and denote $PP(\boldsymbol{u}^{n+1,\text{pre}})$ as the new solution modified by the positivity-preserving limiter. Now we give the flow chart of our high-order entropy stable and positivity-preserving DG scheme with the Euler forward time discretization,

1. Use the DG scheme (2.10) to obtain $\boldsymbol{F}(\boldsymbol{u}^n)$,
2. Calculate $\boldsymbol{u}^{n+1,\text{pre}} = \boldsymbol{u}^n + \tau\boldsymbol{F}(\boldsymbol{u}^n)$ and the cell averages $\bar{\boldsymbol{u}}^{n+1,\text{pre}}$,
3. Utilize the positivity-preserving limiter to get $\boldsymbol{u}^{n+1} = PP(\boldsymbol{u}^{n+1,\text{pre}})$.

In order to obtain high-order accuracy both in space and time, we adopt the third-order strong stability-preserving Runge-Kutta (SSP-RK) methods [16] for the time discretization. To be specific, the following third-order SSP-RK scheme will be used,

$$\begin{aligned}\boldsymbol{u}^{(1),\text{pre}} &= \boldsymbol{u}^n + \tau\boldsymbol{F}(\boldsymbol{u}^n),\\ \boldsymbol{u}^{(1)} &= PP(\boldsymbol{u}^{(1),\text{pre}}),\\ \boldsymbol{u}^{(2),\text{pre}} &= \tfrac{3}{4}\boldsymbol{u}^n + \tfrac{1}{4}\left(\boldsymbol{u}^{(1)} + \tau\boldsymbol{F}(\boldsymbol{u}^{(1)})\right),\\ \boldsymbol{u}^{(2)} &= PP(\boldsymbol{u}^{(2),\text{pre}}),\\ \boldsymbol{u}^{n+1,\text{pre}} &= \tfrac{1}{3}\boldsymbol{u}^n + \tfrac{2}{3}\left(\boldsymbol{u}^{(2)} + \tau\boldsymbol{F}(\boldsymbol{u}^{(2)})\right),\\ \boldsymbol{u}^{n+1} &= PP(\boldsymbol{u}^{n+1,\text{pre}}).\end{aligned} \tag{2.31}$$

Remark 2.2. *Since the SSP-RK time discretization methods can be regarded as a convex combination of the Euler forward methods and the solution preserves positivity with the scaling positivity-preserving limiter (2.29) under the time step condition (2.24), consequently, we get a positivity-preserving higher order scheme for the model (2.1).*

Remark 2.3. *The DG scheme (2.25) can be written as*

$$\frac{h}{2}\mathcal{M}\frac{\boldsymbol{u}^{pre}-\boldsymbol{u}^{n}}{\tau} = \mathcal{D}_u\boldsymbol{Q}, \tag{2.32}$$

$$\left(\mathcal{I}-\frac{4\lambda}{h^2}\mathcal{M}^{-1}\mathcal{D}_d\mathcal{M}^{-1}\mathcal{D}_u\right)\boldsymbol{Q} = \frac{2}{h}\mathcal{M}^{-1}\mathcal{D}_d\boldsymbol{k}. \tag{2.33}$$

When we solve this DG scheme, we will first solve the heat flux $\boldsymbol{Q}$ by the linear system (2.33). Then we will use the known $\boldsymbol{Q}$ to solve $\boldsymbol{u}^{pre}$ by the first equation (2.32). Although the size of the matrix $\left(\mathcal{I}-\frac{4\lambda}{h^2}\mathcal{M}^{-1}\mathcal{D}_d\mathcal{M}^{-1}\mathcal{D}_u\right)$ is $(m+1)N\times(m+1)N$, it is a diagonally dominant matrix and independent of time, hence solving the linear system does not bring too much difficulty.

3 High-order entropy stable and positivity-preserving DG scheme for the two-dimensional nonlocal electron heat transport model

3.1 The stability property for the two-dimensional nonlocal electron heat transport model

In this section, we consider the nonlocal electron heat transport model (1.1) in the two-dimensional case,

$$\begin{aligned} \frac{\partial u}{\partial t} &= -\frac{\partial Q_1}{\partial x}-\frac{\partial Q_2}{\partial y} \\ Q_1 &= -k(u)_x+\lambda\left(\frac{\partial^2 Q_1}{\partial x^2}+\frac{\partial^2 Q_1}{\partial y^2}\right) \\ Q_2 &= -k(u)_y+\lambda\left(\frac{\partial^2 Q_2}{\partial x^2}+\frac{\partial^2 Q_2}{\partial y^2}\right) \end{aligned} \tag{3.1}$$

where $\vec{Q}=\binom{Q_1}{Q_2}$ is the electron heat flux. Similar to the one-dimensional case, we take a convex function $U(u)$, such that $U'(u)=k(u)$ and the entropy function is $E=\int_\Omega U dxdy$.

Then we can show that the total entropy is non-increasing with respect to time,

$$\begin{aligned}\frac{dE}{dt} =& \int_\Omega k(u)u_t dxdy \\ =& \int_\Omega k(u)u_t dxdy + \int_\Omega \left[-k(u)_x Q_1 - Q_1^2 + \lambda Q_1 \Delta Q_1\right] dxdy \\ &+ \int_\Omega \left[-k(u)_y Q_2 - Q_2^2 + \lambda Q_2 \Delta Q_2\right] dxdy \\ =& -\int_\Omega \left[\partial_x(k(u)Q_1) + \partial_y(k(u)Q_2)\right] dxdy - \int_\Omega \left(Q_1^2 + Q_2^2\right) dxdy \\ &- \lambda \int_\Omega \left[\left|\frac{\partial Q_1}{\partial x}\right|^2 + \left|\frac{\partial Q_1}{\partial y}\right|^2 + \left|\frac{\partial Q_2}{\partial x}\right|^2 + \left|\frac{\partial Q_2}{\partial y}\right|^2\right] dxdy \\ \leq& 0.\end{aligned} \tag{3.2}$$

Here the periodic or compactly supported boundary condition is applied. The Fourier analysis for the one-dimensional case can be extended to multi-dimensional cases, so we do not repeat it here. From the Fourier analysis we know that the solution u of the model (3.1) is stable with $k(u) = u$ and the periodic boundary condition.

3.2 Two-dimensional semi-discrete DG scheme for the nonlocal electron heat transport model

By introducing the new variables $G_l,\ l = 1, 2, 3, 4$, we rewrite the original equation (3.1) as

$$\begin{cases} \partial_t u &= -\partial_x Q_1 - \partial_y Q_2 \\ Q_1 &= -\lambda(\partial_x G_1 + \partial_y G_2) - \partial_x k(u) \\ Q_2 &= -\lambda(\partial_x G_3 + \partial_y G_4) - \partial_y k(u) \\ G_1 &= -\partial_x Q_1, \quad G_2 = -\partial_y Q_1 \\ G_3 &= -\partial_x Q_2, \quad G_4 = -\partial_y Q_2 \\ u(x, y, 0) &= u^0(x, y) \end{cases} \tag{3.3}$$

where $\lambda \geq 0, k'(u) > 0$ and there is no second order derivative terms in the system (3.3). Suppose Ω is a rectangular domain and consider the following regular partition $\Omega := \bigcup_{i=1,j=1}^{N_x,N_y} R_{i,j},\ R_{i,j} := I_i \times J_j$,

$$\begin{aligned} I_i &= \left[x_{i-\frac{1}{2}}, x_{i+\frac{1}{2}}\right], \quad x_{\frac{1}{2}} < x_{\frac{3}{2}} <, \cdots, < x_{N_x+\frac{1}{2}}, \quad h_i^x = x_{i+\frac{1}{2}} - x_{i-\frac{1}{2}}, \\ J_j &= \left[y_{j-\frac{1}{2}}, y_{j+\frac{1}{2}}\right], \quad y_{\frac{1}{2}} < y_{\frac{3}{2}} <, \cdots, < y_{N_y+\frac{1}{2}}, \quad h_j^y = y_{j+\frac{1}{2}} - y_{j-\frac{1}{2}}. \end{aligned}$$

The discrete discontinuous Galerkin space of tensor product polynomials of degree m is

$$\mathbf{V}^m = \left\{\mathbf{w}(x, y) : \mathbf{w}(x, y) \mid_{R_{i,j}} \in \mathcal{Q}^m\left(R_{i,j}\right), 1 \leq i \leq N_x, 1 \leq j \leq N_y\right\}.$$

Here, $\mathcal{Q}^m(R_{i,j}) = \{\sum_{k,l\le m} c_{k,l}p_k(x)q_l(y) : p_k, q_l \text{ are polynomials of degree} \le m\}$ is the space of tensor product polynomials of degree m on $R_{i,j}$.

Next we will design a two-dimensional DG scheme to solve the nonlocal electron heat transport model (3.1). We seek the numerical solution $u, Q_1, Q_2, G_1, G_2, G_3, G_4$ from $\mathbf{V}^m$ such that for any smooth test function $\varphi, \psi_1, \psi_2, \phi_1, \phi_2, \phi_3, \phi_4 \in \mathbf{V}^m$ and $1 \le i \le N_x, 1 \le j \le N_y$,

$$
\begin{aligned}
\int_{R_{i,j}} \partial_t u\varphi dxdy &= \int_{R_{i,j}} (Q_1\partial_x\varphi + Q_2\partial_y\varphi)\, dxdy \\
&\quad - \int_{J_j} \left[\hat{Q}_1^x(x_{i+\frac{1}{2}}, y)\varphi(x^-_{i+\frac{1}{2}}, y) - \hat{Q}_1^x(x_{i-\frac{1}{2}}, y)\varphi(x^+_{i-\frac{1}{2}}, y)\right] dy \\
&\quad - \int_{I_i} \left[\hat{Q}_2^y(x, y_{j+\frac{1}{2}})\varphi(x, y^-_{j+\frac{1}{2}}) - \hat{Q}_2^y(x, y_{j-\frac{1}{2}})\varphi(x, y^+_{j-\frac{1}{2}})\right] dx \\
\int_{R_{i,j}} Q_1\psi_1 dxdy &= \int_{R_{i,j}} [(k + \lambda G_1)\partial_x\psi_1 + \lambda G_2\partial_y\psi_1]\, dxdy \\
&\quad - \int_{J_j} (\hat{k}^x + \lambda\hat{G}_1^x)(x_{i+\frac{1}{2}}, y)\psi_1(x^-_{i+\frac{1}{2}}, y)dy \\
&\quad + \int_{J_j} (\hat{k}^x + \lambda\hat{G}_1^x)(x_{i-\frac{1}{2}}, y)\psi_1(x^+_{i-\frac{1}{2}}, y)dy \\
&\quad - \lambda\int_{I_i} \left[\hat{G}_2^y(x, y_{j+\frac{1}{2}})\psi_1(x, y^-_{j+\frac{1}{2}}) - \hat{G}_2^y(x, y_{j-\frac{1}{2}})\psi_1(x, y^+_{j-\frac{1}{2}})\right] dx \\
\int_{R_{i,j}} Q_2\psi_2 dxdy &= \int_{R_{i,j}} [\lambda G_3\partial_x\psi_2 + (k + \lambda G_4)\partial_y\psi_2]\, dxdy \\
&\quad - \lambda\int_{J_j} \left[\hat{G}_3^x(x_{i+\frac{1}{2}}, y)\psi_2(x^-_{i+\frac{1}{2}}, y) - \hat{G}_3^x(x_{i-\frac{1}{2}}, y)\psi_2(x^+_{i-\frac{1}{2}}, y)\right] dy \\
&\quad - \int_{I_i} (\hat{k}^y + \lambda\hat{G}_4^y)(x, y_{j+\frac{1}{2}})\psi_2(x, y^-_{j+\frac{1}{2}})dx \\
&\quad + \int_{I_i} (\hat{k}^y + \lambda\hat{G}_4^y)(x, y_{j-\frac{1}{2}})\psi_2(x, y^+_{j-\frac{1}{2}})dx \\
\int_{R_{i,j}} G_1\phi_1 dxdy &= \int_{R_{i,j}} Q_1\partial_x\phi_1 dxdy \\
&\quad - \int_{J_j} \left[\hat{Q}_1^x(x_{i+\frac{1}{2}}, y)\phi_1(x^-_{i+\frac{1}{2}}, y) - \hat{Q}_1^x(x_{i-\frac{1}{2}}, y)\phi_1(x^+_{i-\frac{1}{2}}, y)\right] dy \\
\int_{R_{i,j}} G_2\phi_2 dxdy &= \int_{R_{i,j}} Q_1\partial_y\phi_2 dxdy \\
&\quad - \int_{I_i} \left[\hat{Q}_1^y(x, y_{j+\frac{1}{2}})\phi_2(x, y^-_{j+\frac{1}{2}}) - \hat{Q}_1^y(x, y_{j-\frac{1}{2}})\phi_2(x, y^+_{j-\frac{1}{2}})\right] dx \\
\int_{R_{i,j}} G_3\phi_3 dxdy &= \int_{R_{i,j}} Q_2\partial_x\phi_3 dxdy \\
&\quad - \int_{J_j} \left[\hat{Q}_2^x(x_{i+\frac{1}{2}}, y)\phi_3(x^-_{i+\frac{1}{2}}, y) - \hat{Q}_2^x(x_{i-\frac{1}{2}}, y)\phi_3(x^+_{i-\frac{1}{2}}, y)\right] dy \\
\int_{R_{i,j}} G_4\phi_4 dxdy &= \int_{R_{i,j}} Q_2\partial_y\phi_4 dxdy \\
&\quad - \int_{I_i} \left[\hat{Q}_2^y(x, y_{j+\frac{1}{2}})\phi_4(x, y^-_{j+\frac{1}{2}}) - \hat{Q}_2^y(x, y_{j-\frac{1}{2}})\phi_4(x, y^+_{j-\frac{1}{2}})\right] dx
\end{aligned}
\tag{3.4}
$$

where we denote $k(u)$ as k, for simplicity. $\hat{Q}_1^x, \hat{Q}_2^x, \hat{k}^x, \hat{G}_1^x, \hat{G}_3^x$ are the numerical fluxes in the x direction, $\hat{Q}_1^y, \hat{Q}_2^y, \hat{k}^y, \hat{G}_2^y, \hat{G}_4^y$ are the numerical fluxes in the y direction. In this paper, we

adopt the alternative numerical flux for the two-dimensional DG scheme

$$\begin{array}{rclrcl}
\hat{Q}_1^x(x_{i-\frac{1}{2}}, y_j(\eta_s)) &=& Q_1(x_{i-\frac{1}{2}}^-, y_j(\eta_s)), & \hat{Q}_1^y(x_i(\xi_r), y_{j-\frac{1}{2}}) &=& Q_1(x_i(\xi_r), y_{j-\frac{1}{2}}^-), \\
\hat{Q}_2^x(x_{i-\frac{1}{2}}, y_j(\eta_s)) &=& Q_2(x_{i-\frac{1}{2}}^-, y_j(\eta_s)), & \hat{Q}_2^y(x_i(\xi_r), y_{j-\frac{1}{2}}) &=& Q_2(x_i(\xi_r), y_{j-\frac{1}{2}}^-), \\
\hat{k}^x(x_{i-\frac{1}{2}}, y_j(\eta_s)) &=& k(x_{i-\frac{1}{2}}^+, y_j(\eta_s)), & \hat{k}^y(x_i(\xi_r), y_{j-\frac{1}{2}}) &=& k(x_i(\xi_r), y_{j-\frac{1}{2}}^+), \\
\hat{G}_1^x(x_{i-\frac{1}{2}}, y_j(\eta_s)) &=& G_1(x_{i-\frac{1}{2}}^+, y_j(\eta_s)), & \hat{G}_2^y(x_i(\xi_r), y_{j-\frac{1}{2}}) &=& G_2(x_i(\xi_r), y_{j-\frac{1}{2}}^+), \\
\hat{G}_3^x(x_{i-\frac{1}{2}}, y_j(\eta_s)) &=& G_3(x_{i-\frac{1}{2}}^+, y_j(\eta_s)), & \hat{G}_4^y(x_i(\xi_r), y_{j-\frac{1}{2}}) &=& G_4(x_i(\xi_r), y_{j-\frac{1}{2}}^+).
\end{array} \tag{3.5}$$

Here we apply the Gauss-Lobatto quadrature rule on the rectangular meshes with $(m+1)^2$ quadrature points $\{(x_i(\xi_r), y_j(\eta_s))\}_{r=0,s=0}^{m,m}$ on each cell $R_{i,j}$,

$$\begin{array}{rcl}
x_i(\xi_r) &:=& \frac{1}{2}(x_{i-\frac{1}{2}} + x_{i+\frac{1}{2}}) + \frac{\xi_r}{2} h_i^x, \\
y_j(\eta_s) &:=& \frac{1}{2}(y_{j-\frac{1}{2}} + y_{j+\frac{1}{2}}) + \frac{\eta_s}{2} h_j^y,
\end{array}$$

where (ξ_r, η_s) is the quadrature point on the reference cell $R := I \times J = [-1, 1] \times [-1, 1]$, and the corresponding quadrature weight is $\omega_r \omega_s$, where the definition of $\{\omega_r\}_{r=0}^m$, $\{\omega_s\}_{s=0}^m$ is the same as that in the one-dimensional case.

Following the notations in Section 2.1, we define the two-dimensional Lagrangian nodal basis polynomials

$$\mathcal{L}_{rs}(\xi, \eta) = L_r(\xi) L_s(\eta) = \prod_{l=0, l\neq r}^{m} \frac{\xi - \xi_l}{\xi_r - \xi_l} \prod_{l=0, l\neq s}^{m} \frac{\eta - \eta_l}{\eta_s - \eta_l}.$$

To distinguish from the matrices defined in Section 2, we use bold letters to represent the matrices in the two-dimensional case. Define the $(m+1)^2 \times (m+1)^2$ matrix

$$\boldsymbol{V} = [\vec{L}_{00}, \cdots, \vec{L}_{0m}, \vec{L}_{10}, \cdots, \vec{L}_{1m}, \cdots, \vec{L}_{mm}],$$

where

$$\vec{L}_{rs} = (\mathcal{L}_{rs}(\xi_0, \eta_0), \cdots, \mathcal{L}_{rs}(\xi_0, \eta_m), \mathcal{L}_{rs}(\xi_1, \eta_0), \cdots, \mathcal{L}_{rs}(\xi_1, \eta_m), \cdots, \mathcal{L}_{rs}(\xi_m, \eta_m))^T$$

are the values of basis polynomials $\mathcal{L}_{rs}(\xi, \eta)$ at each quadrature point. Here all the quadrature points are arranged in a certain order. Notice that the different arrangement orders will lead to different difference matrices, mass matrices, stiffness matrices, and so on. Define the matrices

$$\begin{aligned}
\boldsymbol{V}^x &= [\partial_x \vec{L}_{00}, \cdots, \partial_x \vec{L}_{0m}, \partial_x \vec{L}_{10}, \cdots, \partial_x \vec{L}_{1m}, \cdots, \partial_x \vec{L}_{mm}], \\
\boldsymbol{V}^y &= [\partial_y \vec{L}_{00}, \cdots, \partial_y \vec{L}_{0m}, \partial_y \vec{L}_{10}, \cdots, \partial_y \vec{L}_{1m}, \cdots, \partial_y \vec{L}_{mm}],
\end{aligned}$$

then the two-dimensional discrete difference matrices $\boldsymbol{D}^x, \boldsymbol{D}^y$ can be written as

$$\boldsymbol{D}^x \boldsymbol{V} = \boldsymbol{V}^x, \quad \boldsymbol{D}^y \boldsymbol{V} = \boldsymbol{V}^y.$$

The operators $\boldsymbol{D}^x, \boldsymbol{D}^y$ transform point values to derivatives at the related points and they can be calculated by Kronecker product

$$\boldsymbol{D}^x = D \bigotimes I, \quad \boldsymbol{D}^y = I \bigotimes D,$$

where I is an identity matrix of the size $(m+1)\times(m+1)$. Then we have the two-dimensional diagonal mass matrix $\boldsymbol{M} = \text{diag}\{\omega_0\omega_0, \cdots, \omega_0\omega_m, \omega_1\omega_0, \cdots, \omega_1\omega_m, \cdots, \omega_m\omega_m\}$, stiffness matrices $\boldsymbol{S}^x := \boldsymbol{M}\boldsymbol{D}^x, \boldsymbol{S}^y := \boldsymbol{M}\boldsymbol{D}^y$, and boundary matrices

$$\begin{aligned} \boldsymbol{B}^x &:= \text{diag}\{\tau_{00}^x, \cdots, \tau_{0m}^x, \tau_{10}^x, \cdots, \tau_{1m}^x, \cdots, \tau_{mm}^x\} = \boldsymbol{S}^x + \boldsymbol{S}^{x,T}, \\ \boldsymbol{B}^y &:= \text{diag}\{\tau_{00}^y, \cdots, \tau_{0m}^y, \tau_{10}^y, \cdots, \tau_{1m}^y, \cdots, \tau_{mm}^y\} = \boldsymbol{S}^y + \boldsymbol{S}^{y,T}, \end{aligned} \tag{3.6}$$

where $\text{diag}\{\vec{x}\}$ represents a diagonal matrix with the vector $\vec{x}$ as the diagonal elements.

We can also give the following two-dimensional summation-by-parts properties

Lemma 3.1. *According to the definition of the above matrices, we have the following two-dimensional summation-by-parts properties which are the discrete analogues of the integration-by-parts properties. Denote* $diag(\boldsymbol{M}) = \{\tilde{\omega}_{\tilde{r}}\}_{\tilde{r}=1}^{(m+1)^2}$, $diag(\boldsymbol{B}^x) = \{\tilde{\tau}_{\tilde{r}}^x\}_{\tilde{r}=1}^{(m+1)^2}$, $diag(\boldsymbol{B}^y) = \{\tilde{\tau}_{\tilde{r}}^y\}_{\tilde{r}=1}^{(m+1)^2}$, *so we have*

1) $\boldsymbol{S}^x = \boldsymbol{M}\boldsymbol{D}^x, \quad \boldsymbol{M}\boldsymbol{D}^x + \boldsymbol{D}^{x,T}\boldsymbol{M} = \boldsymbol{S}^x + \boldsymbol{S}^{x,T} = \boldsymbol{B}^x,$

$\boldsymbol{S}^y = \boldsymbol{M}\boldsymbol{D}^y, \quad \boldsymbol{M}\boldsymbol{D}^y + \boldsymbol{D}^{y,T}\boldsymbol{M} = \boldsymbol{S}^y + \boldsymbol{S}^{y,T} = \boldsymbol{B}^y,$

2) $\sum_{\tilde{l}=1}^{(m+1)^2} \boldsymbol{D}_{\tilde{r}\tilde{l}}^x = \sum_{\tilde{l}=1}^{(m+1)^2} \boldsymbol{D}_{\tilde{r}\tilde{l}}^y = 0,\ 1 \le \tilde{r} \le (m+1)^2,$

3) $\sum_{\tilde{l}=1}^{(m+1)^2} \boldsymbol{S}_{\tilde{r}\tilde{l}}^x = \sum_{\tilde{l}=1}^{(m+1)^2} \tilde{\omega}_{\tilde{r}} \boldsymbol{D}_{\tilde{r}\tilde{l}}^x = 0,\ 1 \le \tilde{r} \le (m+1)^2,$

$\sum_{\tilde{l}=1}^{(m+1)^2} \boldsymbol{S}_{\tilde{r}\tilde{l}}^y = \sum_{\tilde{l}=1}^{(m+1)^2} \tilde{\omega}_{\tilde{r}} \boldsymbol{D}_{\tilde{r}\tilde{l}}^y = 0,\ 1 \le \tilde{r} \le (m+1)^2,$

4) $\sum_{\tilde{l}=1}^{(m+1)^2} \boldsymbol{S}_{\tilde{l}\tilde{r}}^x = \tilde{\tau}_{\tilde{r}}^x, \quad \sum_{\tilde{l}=1}^{(m+1)^2} \boldsymbol{S}_{\tilde{l}\tilde{r}}^y = \tilde{\tau}_{\tilde{r}}^y,\ 1 \le \tilde{r} \le (m+1)^2.$

The proof of Lemma 3.1 is straightforward based on the proof of Lemma 2.1. So we omit it here to save space. Then we can use the quadrature rule to substitute the integral in the DG scheme (3.4). For simplicity, we denote $\vec{u}^{i,j}, \vec{Q}_1^{i,j}, \vec{Q}_2^{i,j}, \vec{k}^{i,j}, \vec{G}_1^{i,j}, \vec{G}_2^{i,j}, \vec{G}_3^{i,j}, \vec{G}_4^{i,j}$ to be the values at the Gauss-Lobatto quadrature points arranged by the same order

$$\begin{aligned}\vec{u}^{i,j} :=&[u_1^{i,j}, u_2^{i,j}, \cdots, u_{\tilde{r}}^{i,j}, \cdots, u_{(m+1)^2}^{i,j}]^T \\ =&[u(x_i(\xi_0), y_j(\eta_0)), \cdots, u(x_i(\xi_0), y_j(\eta_m)), u(x_i(\xi_1), y_j(\eta_0)), \cdots, u(x_i(\xi_m), y_j(\eta_m))]^T\end{aligned}$$

and define the numerical flux $\vec{Q}_1^{x,i,j,*}$,$\vec{Q}_1^{y,i,j,*}$,$\vec{Q}_2^{x,i,j,*}$,$\vec{Q}_2^{y,i,j,*}$,$\vec{k}^{x,i,j,*}$,$\vec{k}^{y,i,j,*}$,$\vec{G}_1^{x,i,j,*}$,$\vec{G}_2^{y,i,j,*}$,$\vec{G}_3^{x,i,j,*}$,$\vec{G}_4^{y,i,j,*}$ as

$$\vec{Q}_1^{x,i,j,*} = \begin{pmatrix} \hat{Q}_1(x_{i-\frac{1}{2}}, y_j(\eta_0)) \\ 0 \\ \vdots \\ \hat{Q}_1(x_{i+\frac{1}{2}}, y_j(\eta_0)) \\ \hat{Q}_1(x_{i-\frac{1}{2}}, y_j(\eta_1)) \\ 0 \\ \vdots \\ \hat{Q}_1(x_{i+\frac{1}{2}}, y_j(\eta_1)) \\ \vdots \\ \hat{Q}_1(x_{i-\frac{1}{2}}, y_j(\eta_m)) \\ 0 \\ \vdots \\ \hat{Q}_1(x_{i+\frac{1}{2}}, y_j(\eta_m)) \end{pmatrix} \quad \hat{Q}_1^{y,i,j,*} = \begin{pmatrix} \hat{Q}_1(x_i(\xi_0), y_{j-\frac{1}{2}}) \\ \hat{Q}_1(x_i(\xi_1), y_{j-\frac{1}{2}}) \\ \vdots \\ \hat{Q}_1(x_i(\xi_{m-1}), y_{j-\frac{1}{2}}) \\ \hat{Q}_1(x_i(\xi_m), y_{j-\frac{1}{2}}) \\ 0 \\ \vdots \\ 0 \\ \hat{Q}_1(x_i(\xi_0), y_{j+\frac{1}{2}}) \\ \hat{Q}_1(x_i(\xi_1), y_{j+\frac{1}{2}}) \\ \vdots \\ \hat{Q}_1(x_i(\xi_{m-1}), y_{j+\frac{1}{2}}) \\ \hat{Q}_1(x_i(\xi_m), y_{j+\frac{1}{2}}) \end{pmatrix}.$$

Since $\varphi, \psi_1, \psi_2, \phi_1, \phi_2, \phi_3, \phi_4 \in \mathbf{V}_h^m$ can be arbitrary chosen, we apply the two-dimensional summation-by-parts properties for $1 \le i \le N_x,\ 1 \le j \le N_y$ to get our two-dimensional

semi-discrete DG scheme,

$$
\begin{aligned}
\frac{h_i^x h_j^y}{4}\frac{d\vec{u}^{i,j}}{dt} =& \frac{h_j^y}{2}\left(\boldsymbol{M}^{-1}\boldsymbol{D}^{x,T}\boldsymbol{M}\vec{Q}_1^{i,j} - \boldsymbol{M}^{-1}\boldsymbol{B}^x\vec{Q}_1^{x,i,j,*}\right) + \frac{h_i^x}{2}\left(\boldsymbol{M}^{-1}\boldsymbol{D}^{y,T}\boldsymbol{M}\vec{Q}_2^{i,j} - \boldsymbol{M}^{-1}\boldsymbol{B}^y\vec{Q}_2^{y,i,j,*}\right),\\
\frac{h_i^x h_j^y}{4}\vec{Q}_1^{i,j} =& \lambda\frac{h_j^y}{2}\left(\boldsymbol{M}^{-1}\boldsymbol{D}^{x,T}\boldsymbol{M}\vec{G}_1^{i,j} - \boldsymbol{M}^{-1}\boldsymbol{B}^x\vec{G}_1^{x,i,j,*}\right) + \lambda\frac{h_i^x}{2}\left(\boldsymbol{M}^{-1}\boldsymbol{D}^{y,T}\boldsymbol{M}\vec{G}_2^{i,j} - \boldsymbol{M}^{-1}\boldsymbol{B}^y\vec{G}_2^{y,i,j,*}\right)\\
&+ \frac{h_j^y}{2}\left(\boldsymbol{M}^{-1}\boldsymbol{D}^{x,T}\boldsymbol{M}\vec{k}^{i,j} - \boldsymbol{M}^{-1}\boldsymbol{B}^x\vec{k}^{x,i,j,*}\right),\\
\frac{h_i^x h_j^y}{4}\vec{Q}_2^{i,j} =& \lambda\frac{h_j^y}{2}\left(\boldsymbol{M}^{-1}\boldsymbol{D}^{x,T}\boldsymbol{M}\vec{G}_3^{i,j} - \boldsymbol{M}^{-1}\boldsymbol{B}^x\vec{G}_3^{x,i,j,*}\right) + \lambda\frac{h_i^x}{2}\left(\boldsymbol{M}^{-1}\boldsymbol{D}^{y,T}\boldsymbol{M}\vec{G}_4^{i,j} - \boldsymbol{M}^{-1}\boldsymbol{B}^y\vec{G}_4^{y,i,j,*}\right)\\
&+ \frac{h_i^x}{2}\left(\boldsymbol{M}^{-1}\boldsymbol{D}^{y,T}\boldsymbol{M}\vec{k}^{i,j} - \boldsymbol{M}^{-1}\boldsymbol{B}^y\vec{k}^{y,i,j,*}\right),\\
\frac{h_i^x}{2}\vec{G}_1^{i,j} =& \boldsymbol{M}^{-1}\boldsymbol{D}^{x,T}\boldsymbol{M}\vec{Q}_1^{i,j} - \boldsymbol{M}^{-1}\boldsymbol{B}^x\vec{Q}_1^{x,i,j,*},\\
\frac{h_j^y}{2}\vec{G}_2^{i,j} =& \boldsymbol{M}^{-1}\boldsymbol{D}^{y,T}\boldsymbol{M}\vec{Q}_1^{i,j} - \boldsymbol{M}^{-1}\boldsymbol{B}^y\vec{Q}_1^{y,i,j,*},\\
\frac{h_i^x}{2}\vec{G}_3^{i,j} =& \boldsymbol{M}^{-1}\boldsymbol{D}^{x,T}\boldsymbol{M}\vec{Q}_2^{i,j} - \boldsymbol{M}^{-1}\boldsymbol{B}^x\vec{Q}_2^{x,i,j,*},\\
\frac{h_j^y}{2}\vec{G}_4^{i,j} =& \boldsymbol{M}^{-1}\boldsymbol{D}^{y,T}\boldsymbol{M}\vec{Q}_2^{i,j} - \boldsymbol{M}^{-1}\boldsymbol{B}^y\vec{Q}_2^{y,i,j,*}.
\end{aligned}
\tag{3.7}
$$

3.3 Conservative and entropy stable properties of the two-dimensional semi-discrete DG scheme

Following the idea in Section 2.2, we can also prove the above two-dimensional semi-discrete DG scheme (3.7) is conservative for the cell average $\bar{u}^{i,j}$ and satisfies the entropy inequality. The proof of the following two theorems are similar to that for the one-dimensional cases. Hence we omit the proof here to save space.

Theorem 3.1. *Suppose $\vec{u}^{i,j}, \vec{Q}_1^{i,j}, \vec{Q}_2^{i,j}, \vec{k}^{i,j}, \vec{G}_1^{i,j}, \vec{G}_2^{i,j}, \vec{G}_3^{i,j}, \vec{G}_4^{i,j}$ are obtained from the two-dimensional semi-discrete DG scheme (3.7). Under the periodic or compactly supported boundary condition, the cell average $\bar{u}^{i,j}$ in the semi-discrete scheme (3.7) is conservative.*

Theorem 3.2. *Suppose $\vec{u}^{i,j}, \vec{Q}_1^{i,j}, \vec{Q}_2^{i,j}, \vec{k}^{i,j}, \vec{G}_1^{i,j}, \vec{G}_2^{i,j}, \vec{G}_3^{i,j}, \vec{G}_4^{i,j}$ are obtained from the two-dimensional semi-discrete DG scheme (3.7) and E is the associated discrete entropy function. Assume*

the boundary condition is periodic. Then, with the alternative numerical flux (3.5), we have

$$\frac{dE}{dt} = \sum_{i=1}^{N_x}\sum_{j=1}^{N_y}\frac{dE^{i,j}}{dt} = \sum_{i=1}^{N_x}\sum_{j=1}^{N_y}\tilde{\int_{I_i}}\tilde{\int_{J_j}}\frac{dU(u^{i,j})}{dt}dxdy \leq 0.$$

3.4 The positivity-preserving property for the two-dimensional fully discretized DG scheme

If we assume the boundary condition is periodic and the alternative numerical flux is applied, then the two-dimensional semi-discrete DG scheme (3.7) coupled with the Euler forward time discretization can be written as

$$\begin{aligned}
\frac{h_i^x h_j^y}{4}\boldsymbol{M}\frac{\vec{u}^{i,j,\mathrm{pre}}-\vec{u}^{i,j,n}}{\tau} &= \frac{h_j^y}{2}\left(\boldsymbol{D}^{x,T}\boldsymbol{M}\vec{Q}_1^{i,j}-\boldsymbol{B}^x\vec{Q}_1^{x,i,j,*}\right)+\frac{h_i^x}{2}\left(\boldsymbol{D}^{y,T}\boldsymbol{M}\vec{Q}_2^{i,j}-\boldsymbol{B}^y\vec{Q}_2^{y,i,j,*}\right),\\
\frac{h_i^x h_j^y}{4}\boldsymbol{M}\vec{Q}_1^{i,j} &= \lambda\frac{h_j^y}{2}\left(\boldsymbol{D}^{x,T}\boldsymbol{M}\vec{G}_1^{i,j}-\boldsymbol{B}^x\vec{G}_1^{x,i,j,*}\right)+\lambda\frac{h_i^x}{2}\left(\boldsymbol{D}^{y,T}\boldsymbol{M}\vec{G}_2^{i,j}-\boldsymbol{B}^y\vec{G}_2^{y,i,j,*}\right)\\
&\quad+\frac{h_j^y}{2}\left(\boldsymbol{D}^{x,T}\boldsymbol{M}\vec{k}^{i,j}-\boldsymbol{B}^x\vec{k}^{x,i,j,*}\right),\\
\frac{h_i^x h_j^y}{4}\boldsymbol{M}\vec{Q}_2^{i,j} &= \lambda\frac{h_j^y}{2}\left(\boldsymbol{D}^{x,T}\boldsymbol{M}\vec{G}_3^{i,j}-\boldsymbol{B}^x\vec{G}_3^{x,i,j,*}\right)+\lambda\frac{h_i^x}{2}\left(\boldsymbol{D}^{y,T}\boldsymbol{M}\vec{G}_4^{i,j}-\boldsymbol{B}^y\vec{G}_4^{y,i,j,*}\right)\\
&\quad+\frac{h_i^x}{2}\left(\boldsymbol{D}^{y,T}\boldsymbol{M}\vec{k}^{i,j}-\boldsymbol{B}^y\vec{k}^{y,i,j,*}\right),\\
\frac{h_i^x}{2}\boldsymbol{M}\vec{G}_1^{i,j} &= \boldsymbol{D}^{x,T}\boldsymbol{M}\vec{Q}_1^{i,j}-\boldsymbol{B}^x\vec{Q}_1^{x,i,j,*},\\
\frac{h_j^y}{2}\boldsymbol{M}\vec{G}_2^{i,j} &= \boldsymbol{D}^{y,T}\boldsymbol{M}\vec{Q}_1^{i,j}-\boldsymbol{B}^y\vec{Q}_1^{y,i,j,*},\\
\frac{h_i^x}{2}\boldsymbol{M}\vec{G}_3^{i,j} &= \boldsymbol{D}^{x,T}\boldsymbol{M}\vec{Q}_2^{i,j}-\boldsymbol{B}^x\vec{Q}_2^{x,i,j,*},\\
\frac{h_j^y}{2}\boldsymbol{M}\vec{G}_4^{i,j} &= \boldsymbol{D}^{y,T}\boldsymbol{M}\vec{Q}_2^{i,j}-\boldsymbol{B}^y\vec{Q}_2^{y,i,j,*}.
\end{aligned} \tag{3.8}$$

Lemma 3.2. *Consider the linear function $k(u) = u$, the uniform mesh $h = h_i^x = h_j^y$, $\forall i, j$ and the periodic boundary condition. The two-dimensional fully discretized DG scheme (3.8) is stable under the time step condition*

$$\tau \leq \max\{\lambda, \tilde{c}_m h^2\}, \tag{3.9}$$

where $\tilde{c}_m$ is a constant which depends only on the polynomial degree m of the DG space, and its value is $\tilde{c}_m \in (0.001, 0.1)$ determined by the Fourier analysis numerically.

We make the Fourier analysis on the DG scheme (3.8) numerically to verify the stability property with different τ and λ in Figure 3.1 which shows that our DG scheme is stable under

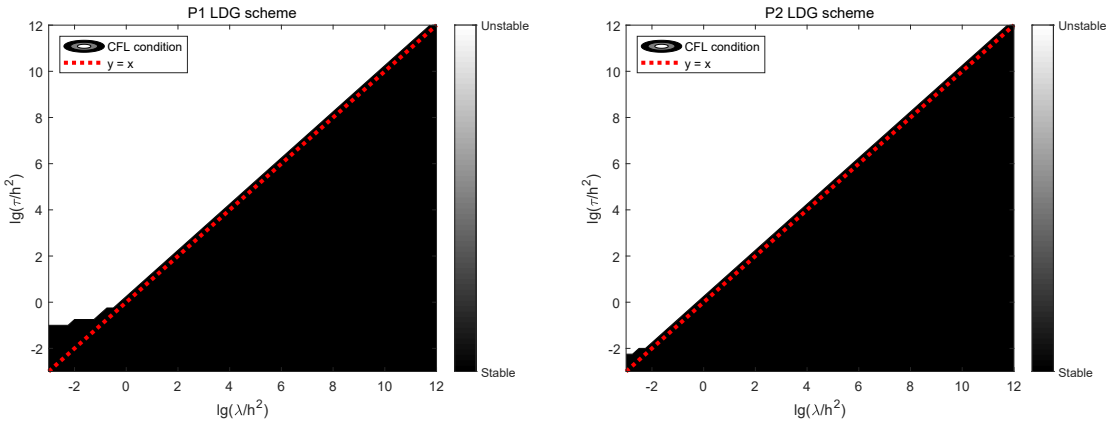

Figure 3.1: The stability region corresponding to the maximum time step τ and the nonlocal parameter λ for the two-dimensional fully discretized DG scheme. The scheme is stable when λ, τ are in the black region. Left: the two-dimensional DG scheme with $m = 1$; Right: the two-dimensional DG scheme with $m = 2$.

such time step condition (3.9). For the local electron heat transport model with $\lambda = 0$, we usually take the stability time step condition as $\tau = \tilde{c}_m h^2$.

We follow the recipe in Section 2.3 and prove the cell averages of the solution obtained from the fully discretized scheme (3.8) are non-negative under the time step condition $\tau \leq \lambda$ and non-negative values at each quadrature point.

Theorem 3.3. *Suppose $k(u)$ is a function with continuous derivative, the mesh is uniform $h = h_i^x = h_j^y$, $\forall i, j$ and the boundary condition is periodic. Suppose the mesh size h is small enough $h < \sqrt{\frac{\lambda}{\tilde{d}_m}}$, where $\tilde{d}_m$ is a constant which depends only on the polynomial degree m of the DG space and its value is $\tilde{d}_m \in [0.01, 0.1]$ determined numerically. Assume $u^n(x_i(\xi_r), y_j(\eta_s)) \geq 0$ at all the quadrature points, then the solution of the fully discretized two-dimensional DG scheme (3.8) satisfies $\bar{u}^{i,j,pre} \geq 0$ under the time step condition*

$$\max_{1\leq i\leq N_x, 1\leq j\leq N_y, 0\leq \xi,\eta\leq m} k'(u^n(x_i(\xi_r), y_j(\eta_s)))\tau \leq \lambda, \tag{3.10}$$

where $\max_{1\leq i\leq N_x, 1\leq j\leq N_y, 0\leq \xi,\eta\leq m} k'(u^n(x_i(\xi_r), y_j(\eta_s)))$ means the maximum value of $k'(u)$ at all of the quadrature points $(x_i(\xi_r), y_j(\eta_s))$.

The proof of Theorem 3.3 is similar to the one-dimensional case, so we skip it here. We also take the values of $\frac{\lambda}{h^2}, \frac{\tau}{h^2}$ from $[10^{-4}, 10^{12}]$ to show the positivity-preserving region in

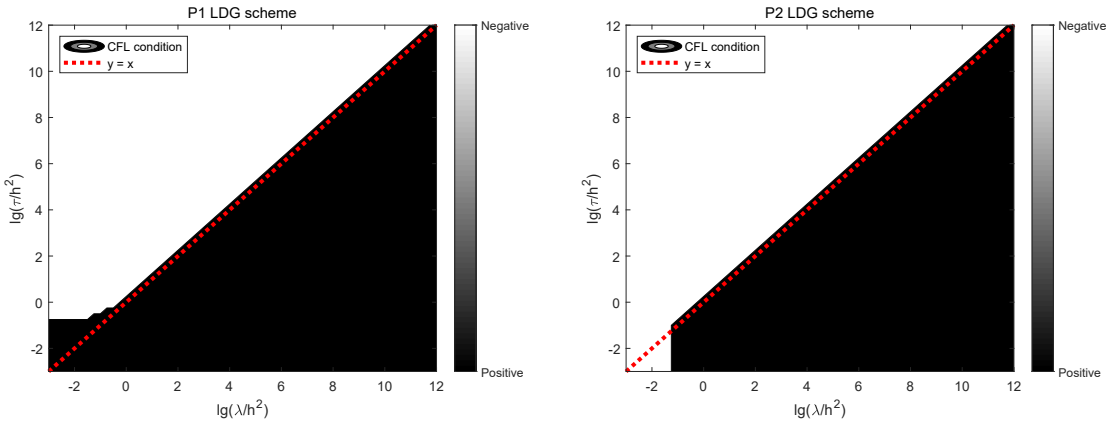

Figure 3.2: The positivity-preserving region corresponding to the maximum time step τ and the nonlocal parameter λ for the two-dimensional DG scheme with the linear function $k(u) = u$. The cell averages $\bar{\boldsymbol{u}}^{\text{pre}}$ can preserve positivity when λ, τ are in the black region. Left: the two-dimensional DG scheme with $m = 1$; Right: the two-dimensional DG scheme with $m = 2$.

Figure 3.2. From Figure 3.2, we know that when $\tau \leq \lambda,\ h < \sqrt{\frac{\lambda}{d_m}}$, the values of the cell average are positive for the linear function $k(u) = u$ on the uniform mesh, and this time the step condition coincides with that for the stability property of our DG scheme which is given in Lemma 3.2. While for $\lambda = 0$, we can always find counterexamples under certain initial condition where negative values of the cell averages appear at the next time step for the model (3.1) with $m \geq 2$.

Similar to the one-dimensional case, we can generalize the above proof to the more general linear case $k(u) = \mu u,\ \mu \geq 0$ and the nonlinear case $k(u) = k'(u)u$. Then the time step condition for $\bar{\boldsymbol{u}}^{\text{pre}} \geq 0$ is

$$\mu\tau \leq \lambda$$

and

$$\max_{1\leq i\leq N_x, 1\leq j\leq N_y, 0\leq \xi,\eta\leq m} k'(u^n(x_i(\xi_r), y_j(\eta_s)))\tau \leq \lambda,$$

respectively.

Based on Theorem 3.3, we can use the positivity-preserving limiter on the two-dimensional DG scheme

$$u^{n+1}(x_i(\xi_r), y_j(\eta_s)) = \bar{u}^{i,j,\text{pre}} + \theta_{i,j}\left(u^{\text{pre}}(x_i(\xi_r), y_j(\eta_s)) - \bar{u}^{i,j,\text{pre}}\right), \quad 0 \leq r, s \leq m,$$

where $\theta_{i,j} = \min\left\{1, \frac{\bar{u}^{i,j,\mathrm{pre}}-\varepsilon}{\bar{u}^{i,j,\mathrm{pre}}-m_{i,j}}\right\}$, $m_{i,j} = \min\limits_{0\le r,s\le m}\{u^{\mathrm{pre}}(x_i(\xi_r), y_j(\eta_s))\}$ and usually we take $\varepsilon = 10^{-16}$ as a small positive number.

We adopt the SSP-RK time discretization method to achieve high-order accuracy in time, thus we obtain the high order entropy stable and positivity-preserving DG scheme (3.8) . The flow chart of our two-dimensional DG scheme is similar to that for the one-dimensional case, so it is omitted for simplicity.

4 Numerical tests

4.1 One-dimensional numerical tests

4.1.1 Accuracy test: Linear local electron heat transport model

Take the linear local electron heat flux $k(u) = u, \lambda = 0$, then the electron heat transport model (2.1) can be written as

$$\begin{cases} \partial_t u &= \partial_{xx} u, \quad x \in [0, 2\pi], \\ u(x,0) &= C + \sin(x), \end{cases} \tag{4.1}$$

where C is a constant. This is a classical linear heat conduction model. With the periodic boundary condition, the problem has an exact solution

$$u(x,t) = C + e^{-t}\sin x.$$

We compute to $T = 0.1$ with the time step $\tau = 0.01h^2$, $h = \min\limits_i h_i$ and the numerical results are listed in Table 4.1. We observe the optimal accuracy for the linear local electron heat transport model for the $\mathcal{P}^2, \mathcal{P}^3, \mathcal{P}^4$ DG schemes.

4.1.2 Accuracy test: Linear nonlocal electron heat transport model with or without the positivity-preserving limiter

Take the linear nonlocal electron heat flux $k(u) = u, \lambda = 0.1$, we consider the initial value problem with a source term $s(x,t)$,

$$\begin{cases} u_t &= -Q_x, \quad x \in [0, 2\pi] \\ Q &= -u_x + \lambda Q_{xx} + s \\ u(x,0) &= C + \sin(x) \\ s(x,t) &= C + \cos(x+t) - (\lambda+1)\sin(x+t), \end{cases} \tag{4.2}$$

Table 4.1: Accuracy test: error and order of the one-dimensional linear local electron heat transport model with the alternative flux (2.5).

	N	L_1 error	order	L_2 error	order	L_∞ error	order
$\mathcal{P}^2$	10	7.7391E-03		4.6334E-03		7.6740E-03	
	20	9.9488E-04	2.96	6.1385E-04	2.92	1.0409E-03	2.88
	40	1.2148E-04	3.03	7.6064E-05	3.01	1.2947E-04	3.01
	80	1.5063E-05	3.01	9.4857E-06	3.00	1.6161E-05	3.00
	120	4.4547E-06	3.00	2.8094E-06	3.00	4.7873E-06	3.00
	N	L_1 error	order	L_2 error	order	L_∞ error	order
$\mathcal{P}^3$	10	2.7205E-04		1.6616E-04		3.0671E-04	
	20	1.6935E-05	4.01	1.0441E-05	3.99	1.8992E-05	4.01
	40	1.0468E-06	4.02	6.4940E-07	4.01	1.1869E-06	4.00
	80	6.5235E-08	4.00	4.0538E-08	4.00	7.4179E-08	4.00
	120	1.2879E-08	4.00	8.0057E-09	4.00	1.4653E-08	4.00
	N	L_1 error	order	L_2 error	order	L_∞ error	order
$\mathcal{P}^4$	10	8.3502E-06		4.9154E-06		8.2568E-06	
	20	2.6061E-07	5.00	1.5241E-07	5.01	2.6257E-07	4.97
	40	8.0977E-09	5.01	4.7522E-09	5.00	8.2399E-09	4.99
	80	2.5274E-10	5.00	1.4843E-10	5.00	2.5848E-10	4.99
	120	3.4506E-11	4.91	1.9914E-11	4.95	3.5562E-11	4.89

where C is a constant. With the periodic boundary condition, the problem has an exact solution

$$\begin{aligned} u(x,t) &= C + \sin(x+t), \\ Q(x,t) &= C - \sin(x+t), \end{aligned} \tag{4.3}$$

where we take $C = 1$. In this problem, the exact solution has a region close to 0 and the numerical solution may become negative. We compute to $T = 1.0$ with the time step $\tau = 0.1h$ for the $\mathcal{P}^2$ DG scheme, $\tau = 0.02h$ for the $\mathcal{P}^3$ DG scheme and $\tau = 0.01h$ for the $\mathcal{P}^4$ DG scheme, where $h = \min_i h_i$. Since we use the third-order SSP-RK method for the DG scheme, we adopt the small time step in the accuracy tests to achieve the optimal accuracy. The numerical results are listed in Table 4.2 for the numerical solution without the positivity-preserving limiter and Table 4.3 for the numerical solution with the positivity-preserving limiter.

The last column $Nc(\%)$ in Table 4.3 is the proportion of quadrature points modified by the positivity-preserving limiter. As one can see, with or without the positivity-preserving

Table 4.2: Accuracy test: error and order of the one-dimensional linear nonlocal electron heat transport model with the alternative numerical flux (2.5) and without the positivity-preserving limiter.

	N	L_1 error	order	L_2 error	order	L_∞ error	order
$\mathcal{P}^2$	10	9.4332E-03		4.8321E-03		6.8979E-03	
	20	1.1351E-03	3.05	5.7952E-04	3.06	8.3442E-04	3.05
	40	1.3880E-04	3.03	7.0916E-05	3.03	1.0240E-04	3.03
	80	1.7166E-05	3.02	8.7717E-06	3.02	1.2603E-05	3.02
	120	5.0694E-06	3.01	2.5900E-06	3.01	3.7166E-06	3.01
	N	L_1 error	order	L_2 error	order	L_∞ error	order
$\mathcal{P}^3$	10	3.0729E-04		1.5952E-04		2.5184E-04	
	20	1.8724E-05	4.04	9.6241E-06	4.05	1.4946E-05	4.07
	40	1.1540E-06	4.02	5.9124E-07	4.02	9.2207E-07	4.02
	80	7.1699E-08	4.01	3.6645E-08	4.01	5.6972E-08	4.02
	120	1.4135E-08	4.00	7.2190E-09	4.01	1.1207E-08	4.01
	N	L_1 error	order	L_2 error	order	L_∞ error	order
$\mathcal{P}^4$	10	8.8605E-06		4.5581E-06		6.5309E-06	
	20	2.7379E-07	5.02	1.3872E-07	5.04	2.0540E-07	4.99
	40	8.4672E-09	5.02	4.2812E-09	5.02	6.2935E-09	5.03
	80	2.6806E-10	4.98	1.3456E-10	4.99	1.8677E-10	5.07
	120	3.7189E-11	4.87	1.8558E-11	4.89	2.2885E-11	5.18

Table 4.3: Accuracy test: error and order of the one-dimensional linear nonlocal electron heat transport model with the alternative numerical flux (2.5) and the positivity-preserving limiter. Nc is the percentage of quadrature points modified by the positivity-preserving limiter

	N	L_1 error	order	L_2 error	order	L_∞ error	order	$Nc(\%)$
$\mathcal{P}^2$	10	9.7937E-03		5.0670E-03		7.8493E-03		1.77E-00
	20	1.1510E-03	3.09	5.9169E-04	3.10	8.7310E-04	3.17	6.45E-01
	40	1.4185E-04	3.02	7.2699E-05	3.02	1.1037E-04	2.98	2.51E-01
	80	2.5484E-05	2.48	1.2134E-05	2.58	3.2487E-05	1.76	1.21E-01
	120	5.3833E-06	3.83	2.8303E-06	3.59	8.5473E-06	3.29	8.63E-02
	N	L_1 error	order	L_2 error	order	L_∞ error	order	$Nc(\%)$
$\mathcal{P}^3$	10	3.0739E-04		1.5944E-04		2.5319E-04		6.33E-02
	20	1.8769E-05	4.03	9.6216E-06	4.05	1.4972E-05	4.08	3.14E-02
	40	1.1573E-06	4.02	5.9166E-07	4.02	9.2243E-07	4.02	1.77E-02
	80	7.1707E-08	4.01	3.6645E-08	4.01	5.6988E-08	4.02	3.44E-03
	120	1.4137E-08	4.00	7.2191E-09	4.01	1.1210E-08	4.01	3.06E-03
	N	L_1 error	order	L_2 error	order	L_∞ error	order	$Nc(\%)$
$\mathcal{P}^4$	10	8.8533E-06		4.5608E-06		6.5648E-06		3.03E-02
	20	2.7415E-07	5.01	1.3875E-07	5.04	2.0469E-07	5.00	5.04E-03
	40	8.4692E-09	5.02	4.2813E-09	5.02	6.2936E-09	5.02	1.26E-03
	80	2.6824E-10	4.98	1.3457E-10	4.99	1.8677E-10	5.07	6.29E-04
	120	3.7199E-11	4.87	1.8578E-11	4.88	2.2885E-11	5.18	4.89E-04

limiter, the convergence rate is optimal for the $\mathcal{P}^3, \mathcal{P}^4$ DG schemes.

4.1.3 Accuracy test: Nonlinear nonlocal electron heat transport model

Take the nonlinear nonlocal electron heat flux $k(u) = \frac{u^2}{2}, \lambda = 0.1$, we consider the initial value problem with a source term $s(x,t)$,

$$\begin{cases} u_t &= -Q_x, \quad x \in [0, 2\pi] \\ Q &= -uu_x + \lambda Q_{xx} + s \\ u(x,0) &= C + \cos(x) \\ s(x,t) &= C + e^{-t}\sin x(\lambda + 1 - C - e^{-t}\cos x), \end{cases} \tag{4.4}$$

where C is a constant. With the periodic boundary condition, the problem has an exact solution

$$\begin{aligned} u(x,t) &= C + e^{-t}\cos x, \\ Q(x,t) &= C + e^{-t}\sin x. \end{aligned} \tag{4.5}$$

We compute to $T = 1.0$ with the time step $\tau = 0.1h$ for the $\mathcal{P}^2$ DG scheme, $\tau = 0.02h$ for the $\mathcal{P}^3$ DG scheme and $\tau = 0.01h$ for the $\mathcal{P}^4$ DG scheme, where $h = \min_i h_i$. The numerical results are listed in Table 4.4.

Above all, our high-order entropy stable and positivity-preserving DG scheme achieves the optimal accuracy in the linear and nonlinear cases for both the local and nonlocal models even with the positivity-preserving limiter. Furthermore, we can also extend this scheme to higher order accuracy with the higher-order Gauss-Lobatto quadrature rules and the higher-order SSP-RK time discretization.

4.1.4 The non-oscillatory test

Let us now consider the initial condition as the step function to verify our DG scheme is non-oscillatory for the discontinuous problem or the large-gradient problem,

$$u(x,0) = \begin{cases} 2 & x < 0.5 \\ 3 & x \geq 0.5 \end{cases} \quad x \in [0,1]. \tag{4.6}$$

We test the nonlocal electron heat transport model with $\lambda = 0, 0.01$ for the linear function $k(u) = u$ and the nonlinear function $k(u) = \frac{u^2}{2}$, respectively. In Figure 4.1, it is obvious that our DG scheme is non-oscillatory for both the local and nonlocal models. We can also see that with the time marching, u gradually changes from the step function to a linear function.

Table 4.4: Accuracy test: error and order of the one-dimensional nonlinear nonlocal electron heat transport model with the alternative numerical flux (2.5).

	N	L_1 error	order	L_2 error	order	L_∞ error	order
$\mathcal{P}^2$	10	2.2088E-03		1.3818E-03		2.5562E-03	
	20	2.6182E-04	3.08	1.6874E-04	3.03	3.1737E-04	3.01
	40	3.2292E-05	3.02	2.0978E-05	3.01	3.8944E-05	3.03
	80	4.0249E-06	3.00	2.6191E-06	3.00	4.8063E-06	3.02
	120	1.1923E-06	3.00	7.7590E-07	3.00	1.4200E-06	3.01
	N	L_1 error	order	L_2 error	order	L_∞ error	order
$\mathcal{P}^3$	10	9.2444E-05		5.3833E-05		1.0058E-04	
	20	5.7250E-06	4.01	3.3232E-06	4.02	6.7294E-06	3.90
	40	3.5640E-07	4.01	2.0709E-07	4.00	4.2852E-07	3.97
	80	2.2324E-08	4.00	1.2937E-08	4.00	2.7033E-08	3.99
	120	4.4214E-09	3.99	2.5566E-09	4.00	5.3726E-09	3.98
	N	L_1 error	order	L_2 error	order	L_∞ error	order
$\mathcal{P}^4$	10	3.8069E-06		2.0788E-06		4.3521E-06	
	20	1.1486E-07	5.05	6.4611E-08	5.01	1.2933E-07	5.07
	40	3.5779E-09	5.00	2.0169E-09	5.00	4.0259E-09	5.01
	80	1.1288E-10	4.99	6.3280E-11	4.99	1.2448E-10	5.02
	120	1.5611E-11	4.88	8.5527E-12	4.94	1.7051E-11	4.90

Figure 4.2 shows the results at the first 5 time steps for the local and nonlocal models, for simplicity, we only show the region near the discontinuity $x \in [0.5, 0.6]$. There are significant differences between the performance of these two models. It can be seen that for the local model when the initial value function has large temperature gradient, the change of temperature distribution u starts from the large gradient nearby and diffuses to both sides. Specifically, at $x = 0.5$, the temperature at the right side decreases and only a small range of points are affected at each time step which can be seen in the top subfigures of Figure 4.2. We observe an obvious effect on the points near the large gradient at the first five time steps. Meanwhile, we can observe the nonlocal effect of the nonlocal model from the bottom subfigures of Figure 4.2. Individually, the temperature u of a large range of points near the large gradient region changes slightly, but the change is not so big which differs from the local model.

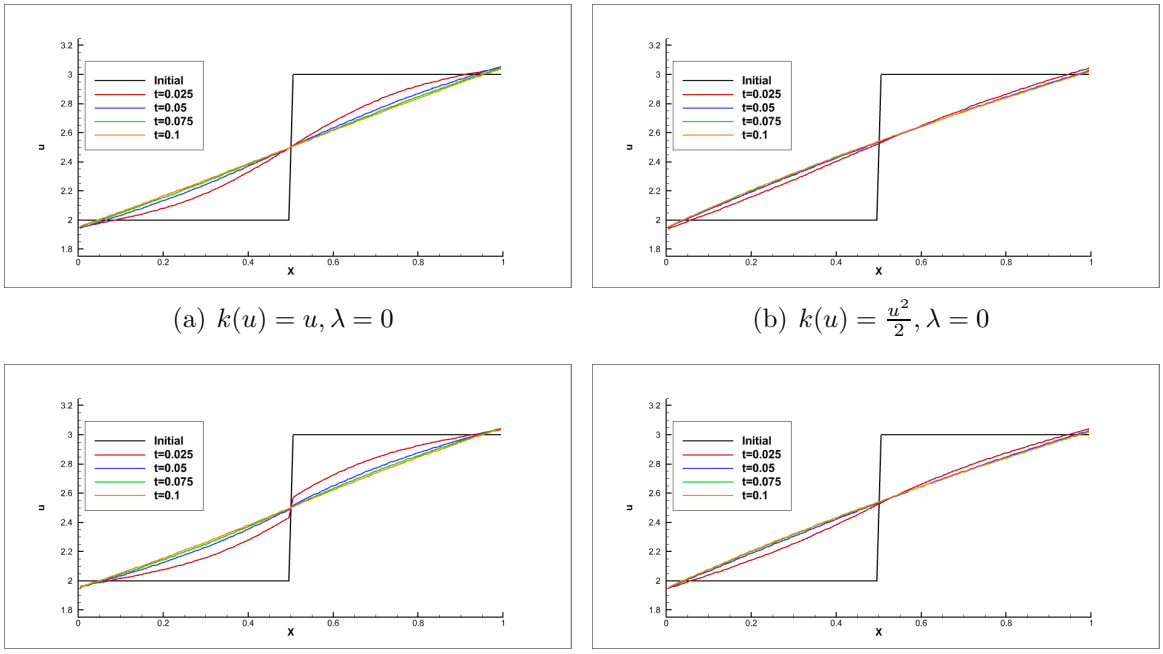

(a) $k(u) = u, \lambda = 0$ (b) $k(u) = \frac{u^2}{2}, \lambda = 0$

(c) $k(u) = u, \lambda = 0.01$ (d) $k(u) = \frac{u^2}{2}, \lambda = 0.01$

Figure 4.1: The non-oscillatory test on the step function (4.6) with the local and nonlocal electron heat transport models at $T = 0.1$. We take the time step condition as $\tau = 0.01h^2$ for $\lambda = 0$ and $\tau = \frac{\lambda}{\max k'(u^0(x_i(\xi_r)))}$ for $\lambda = 0.01$.

4.1.5 The positivity-preserving test

Here, we adopt a new step function

$$u(x,0) = \begin{cases} 1 & 0.245 \le x \le 0.745 \\ 0 & \text{else} \end{cases} \qquad x \in [0,1], \tag{4.7}$$

as the initial function for our linear nonlocal electron heat transport model with $k(u) = u, \lambda = 0.0001$. Notice that we use 100 cells in the numerical test and the $\mathcal{P}^4$ DG numerical scheme. Therefore, we show the numerical result with and without the positivity-preserving limiter near the discontinuity $x \in [0.24, 0.25]$ in Figure 4.3 and Figure 4.4 at the 1st, 5th and 10th time steps respectively.

From the right subfigure of Figure 4.3 and Figure 4.4, we can observe that without the positivity-preserving limiter there are negative values at certain quadrature points near the discontinuity.

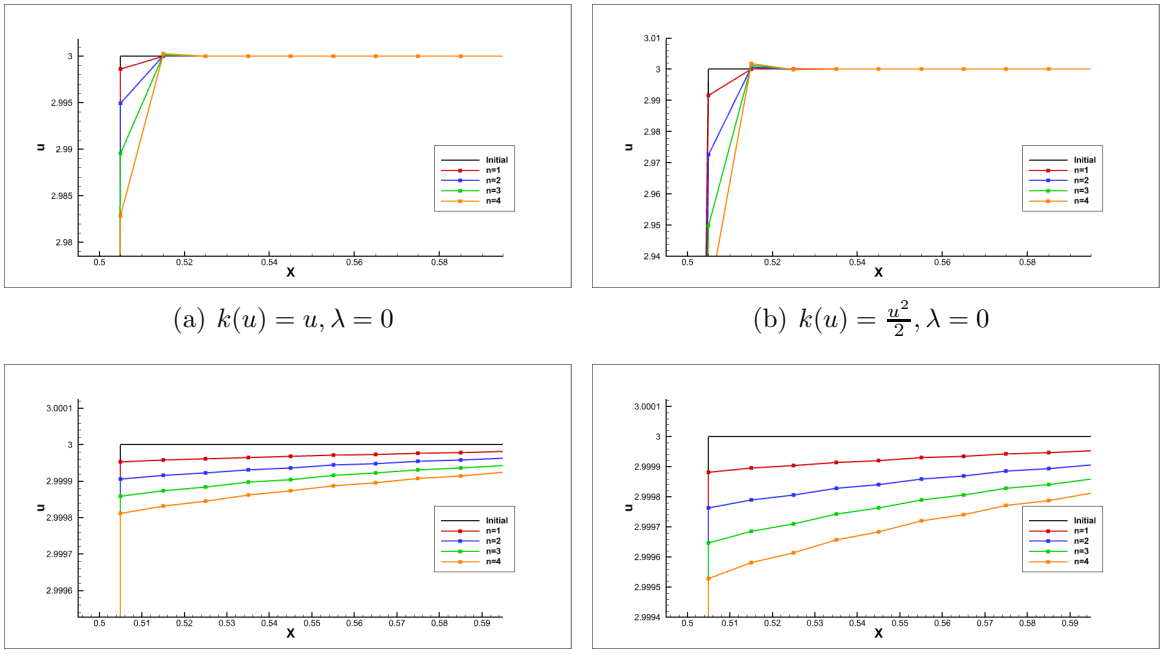

(a) $k(u) = u, \lambda = 0$ (b) $k(u) = \frac{u^2}{2}, \lambda = 0$

(c) $k(u) = u, \lambda = 0.01$ (d) $k(u) = \frac{u^2}{2}, \lambda = 0.01$

Figure 4.2: The first five time steps for the local and nonlocal electron heat transport models with $k(u) = u$ and $k(u) = \frac{u^2}{2}$. We take the time step condition as $\tau = 0.01h^2$ for $\lambda = 0, 0.01$.

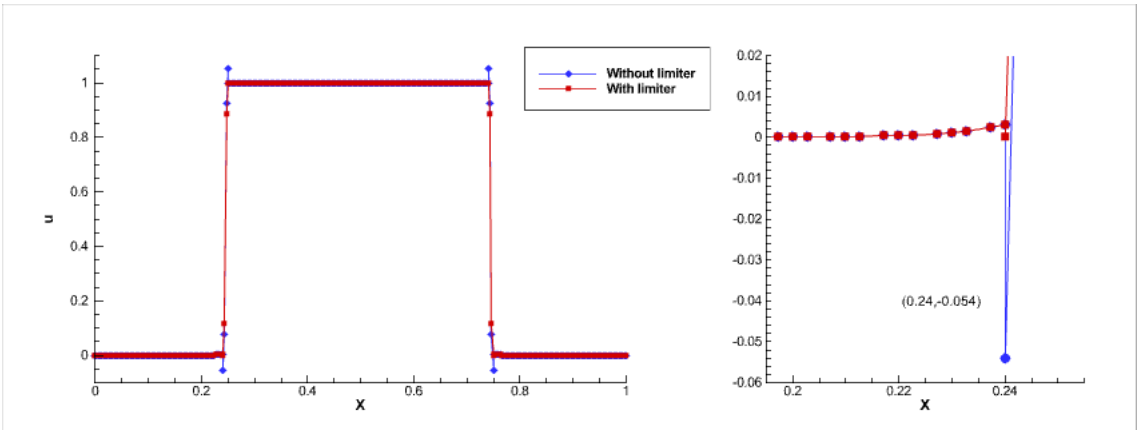

Figure 4.3: The positivity-preserving test on the step function (4.7) with $k(u) = u, \lambda = 0.0001, \tau = 0.02\lambda$. The blue symbol and line are the numerical solution without the positivity-preserving limiter and the red symbol and line are the numerical solution with the positivity-preserving limiter. Left: the numerical solution at the first time step; Right: zoomed-in figure.

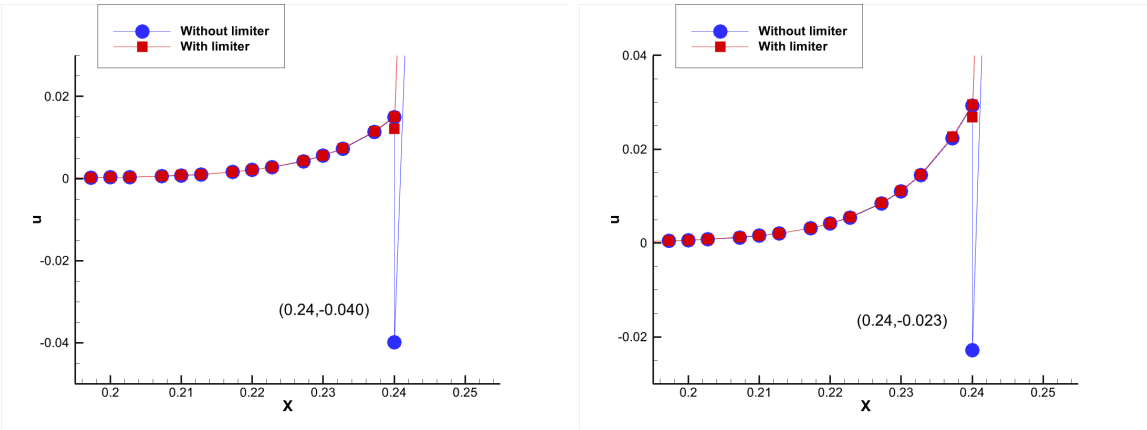

Figure 4.4: The positivity-preserving test on the step function (4.7) with $k(u) = u, \lambda = 0.0001, \tau = 0.02\lambda$. The blue symbol and line are the numerical solution without the positivity-preserving limiter and the red symbol and line are the numerical solution with the positivity-preserving limiter. Left: zoomed-in figure at the 5th time step; Right: zoomed-in figure at the 10th time step.

Besides that, we take the sine function as the initial function

$$u(x, 0) = \sin^4(8\pi x), \quad x \in [0, 1], \tag{4.8}$$

for our linear nonlocal electron heat transport model with $k(u) = u, \lambda = 1 \times 10^{-5}$. We compare the numerical results of the $\mathcal{P}^4$ DG numerical schemes with and without the positivity-preserving limiter at the 1st, 5th and 10th time step.

From the right subfigure of Figure 4.5 and Figure 4.6, we can also observe that without the positivity-preserving limiter there are negative values of quadrature points and our positivity-preserving limiter can handle this problem. Since the negative values of the quadrature points are very close to zero, so there are no significant difference between the numerical results at the first time step in the left subfigure of Figure 4.5.

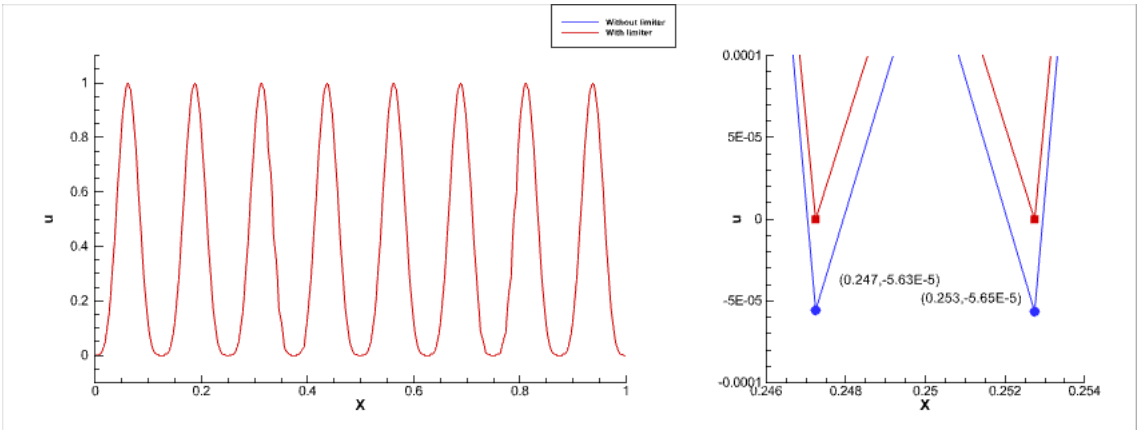

Figure 4.5: The positivity-preserving test on the sine function (4.8) with $k(u) = u, \lambda = 1 \times 10^{-5}, \tau = 0.005\lambda$. The blue symbol and line are the numerical solution without the positivity-preserving limiter and the red symbol and line are the numerical solution with the positivity-preserving limiter. Left: the numerical solution at the first time step; Right: zoomed-in figure.

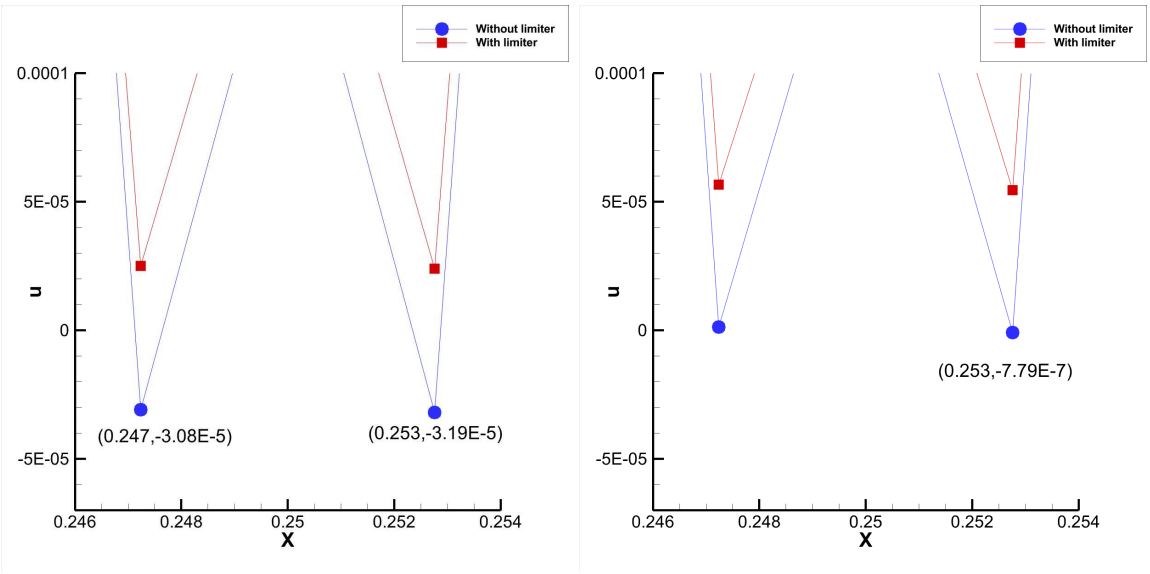

Figure 4.6: The positivity-preserving test on the sine function (4.8) with $k(u) = u, \lambda = 1 \times 10^{-5}, \tau = 0.005\lambda$. The blue symbol and line are the numerical solution without the positivity-preserving limiter and the red symbol and line are the numerical solution with the positivity-preserving limiter. Left: zoomed-in figure at the 5th time step; Right: zoomed-in figure at the 10th time step.

4.1.6 Comparison between the local and nonlocal electron heat transport models

In this subsection, we will compare the different effect between the local and nonlocal models. First, we consider the initial condition as

$$u(x,0) = \begin{cases} C & x < 0.25 \\ C + \sin(4\pi x + \pi) & 0.25 \le x < 0.5 \\ C + 0.1\sin(4\pi x) & 0.5 \le x < 0.75 \\ C & x \ge 0.75 \end{cases} \quad x \in [0,1], \quad C = 0.5, \tag{4.9}$$

for the nonlinear local and nonlocal electron heat transport models with $k(u) = \frac{u^2}{2}, \lambda = 0.02$. Figure 4.7 shows the results for the two electron heat transport models at $T = 0.005$. Intuitively, the temperature at $x = 0.625$ should be reduced first because it is a local maximum, after that, the temperature rises again because there is a very high temperature near $x = 0.375$. Here we only consider a very short time, because the temperature distributions in the two models are very different during this period. As the time marches, the temperature distributions of the two models tend to be the same. For this reason, we can see the numerical solution u of the local model decreases near $x = 0.625$ before $T = 0.005$ from the left subfigure of Figure 4.7. To the opposite, the numerical solution of the nonlocal model with $\lambda = 0.02$ increases near $x = 0.625$ before $T = 0.005$ from the other subfigure of Figure 4.7, which seems to contradict with the common sense. These numerical results can explain the difference between the local and nonlocal electron heat transport model. By this nonlocal model, we can describe the flux reduction and preheat effect due to the nonlocal nature of electron heat transport.

In Figure 4.8, we show the decay of discrete entropy for the function (4.9) with the different models which verifies the stability of discrete entropy in our DG scheme.

The authors in [36] found that the flux limiting effect exists near the high temperature region, while the nonlocal transport of high energy electrons results in a higher energy flux compared to the theoretical prediction by the Spitzer-Harm theory near the low temperature

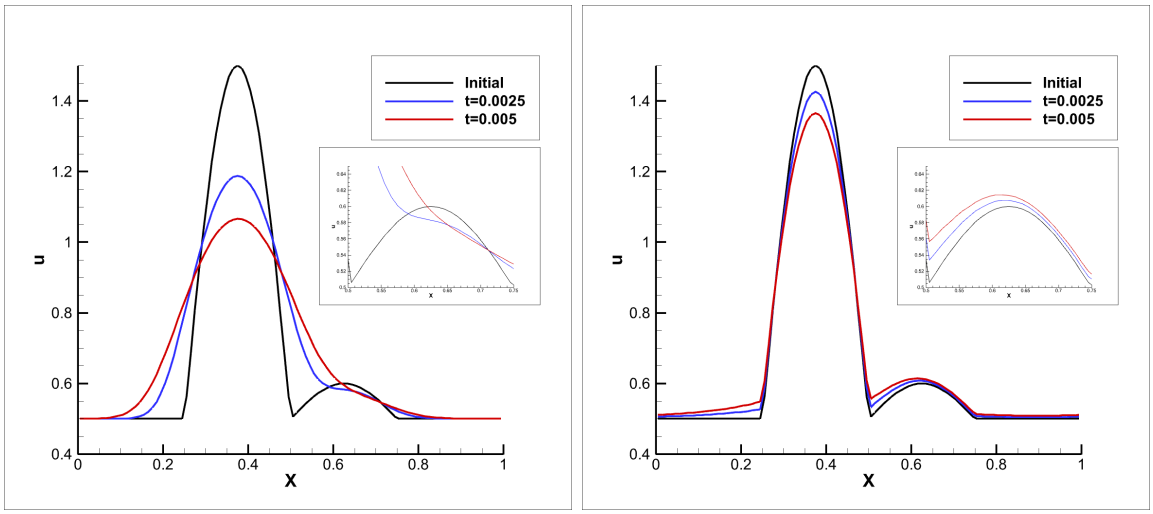

Figure 4.7: The local and nonlocal electron heat transport models at $T = 0.005$. Left: the local model; Right: the nonlocal model.

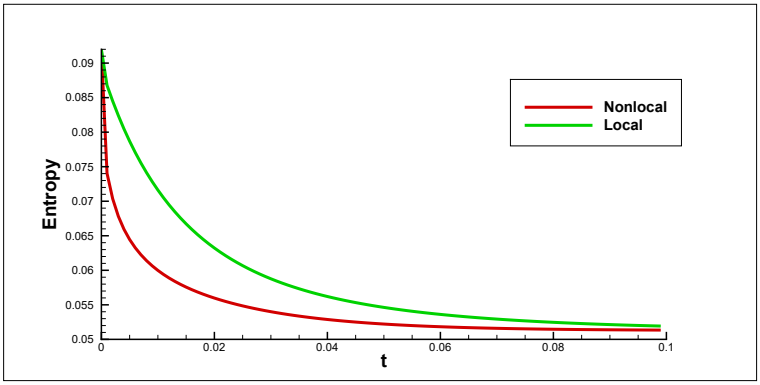

Figure 4.8: The decay of discrete entropy for the function (4.9) of the local and nonlocal models.

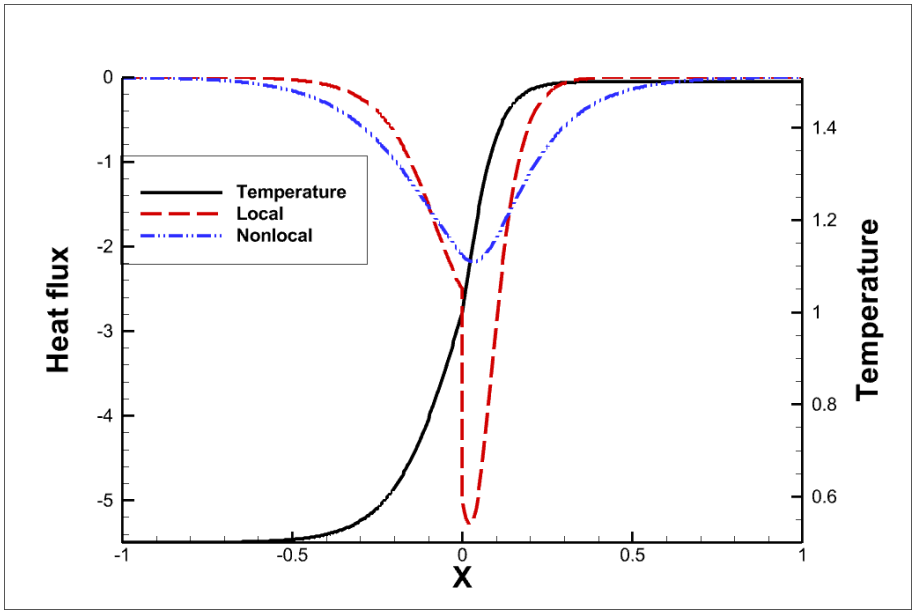

Figure 4.9: Initial temperature condition and the heat flux with the local and nonlocal electron heat transport models, where we take $\lambda = 0.02$.

region. In order to simulate this phenomenon, we design an initial condition of temperature

$$u(x,0) = \begin{cases} C + \frac{1}{1+e^{-10x}} & x < 0 \\ C + \frac{1}{1+e^{-20x}} & x \geq 0 \end{cases} \quad x \in [-1,1], \quad C = 0.5, \tag{4.10}$$

and plot the heat flux Q with the local and nonlocal electron heat transport models at the first time step in Figure 4.9. From this result, we can see our nonlocal electron heat transport model obtains the same qualitative conclusion with the simulation results in [36], where the nonlocal electron heat flux has larger range of influence but lower heat flow than the local electron heat flux.

4.2 Two-dimensional numerical tests

4.2.1 Accuracy test: Linear local electron heat transport model

Take the linear local electron heat flux $k(u) = u, \lambda = 0$, the electron heat transport model (3.1) can be written as

$$\begin{cases} \partial_t u &= \partial_{xx} u + \partial_{yy} u, \quad (x,y) \in [0,2\pi] \times [0,2\pi], \\ u(x,y,0) &= C + \sin(x) + \sin(y), \end{cases} \tag{4.11}$$

where C is a constant. With the periodic boundary condition, the problem has an exact solution

$$u(x, y, t) = C + e^{-t} \left(\sin(x) + \sin(y)\right).$$

We compute to $T = 0.1$ with the time step $\tau = 0.001h^2$, $h = \min_{i,j}\{h_i^x, h_j^y\}$ and the numerical results are listed in Table 4.5 and the optimal accuracy of the $\mathcal{P}^2, \mathcal{P}^3, \mathcal{P}^4$ DG schemes can be observed.

Table 4.5: Accuracy test: error and order of the two-dimensional linear local electron heat transport model with the alternative numerical flux (3.5).

	N_x, N_y	L_1 error	order	L_2 error	order	L_∞ error	order
$\mathcal{P}^2$	10	7.5495E-03		5.2283E-03		1.5348E-02	
	20	9.8295E-04	2.94	6.9266E-04	2.92	2.0818E-03	2.88
	40	1.2126E-04	3.02	8.5829E-05	3.01	2.5894E-04	3.01
	60	3.5829E-05	3.01	2.5387E-05	3.00	7.6644E-05	3.00
	80	1.5100E-05	3.00	1.0703E-05	3.00	3.2322E-05	3.00
	N_x, N_y	L_1 error	order	L_2 error	order	L_∞ error	order
$\mathcal{P}^3$	10	2.6236E-04		1.8749E-04		6.1341E-04	
	20	1.6520E-05	3.99	1.1782E-05	3.99	3.7983E-05	4.01
	40	1.0256E-06	4.01	7.3277E-07	4.01	2.3738E-06	4.00
	60	2.0233E-07	4.00	1.4461E-07	4.00	4.6889E-07	4.00
	80	6.3991E-08	4.00	4.5742E-08	4.00	1.4836E-07	4.00
	N_x, N_y	L_1 error	order	L_2 error	order	L_∞ error	order
$\mathcal{P}^4$	10	8.0304E-06		5.5464E-06		1.6514E-05	
	20	2.4904E-07	5.01	1.7198E-07	5.01	5.2515E-07	4.97
	40	7.7614E-09	5.00	5.3623E-09	5.00	1.6480E-08	4.99
	60	1.0215E-09	5.00	7.0586E-10	5.00	2.1738E-09	5.00

4.2.2 Accuracy test: Linear nonlocal electron heat transport model with or without the positivity-preserving limiter

Take the linear nonlocal electron heat flux $k(u) = u, \lambda = 0.05$, we consider the initial value problem with two source terms $s_1(x, y, t), s_2(x, y, t)$,

$$\begin{cases} \frac{\partial u}{\partial t} &= -\frac{\partial Q_1}{\partial x} - \frac{\partial Q_2}{\partial y}, \quad (x, y) \in [0, 2\pi] \times [0, 2\pi] \\ Q_1 &= -\frac{\partial u}{\partial x} + \lambda(\frac{\partial^2 Q_1}{\partial x^2} + \frac{\partial^2 Q_1}{\partial y^2}) + s_1 \\ Q_2 &= -\frac{\partial u}{\partial y} + \lambda(\frac{\partial^2 Q_2}{\partial x^2} + \frac{\partial^2 Q_2}{\partial y^2}) + s_2 \\ u(x, y, 0) &= C + \sin(x) + \sin(y) \\ s_1(x, y, t) &= C + \cos(x + \alpha t) - \alpha(\lambda + 1)\sin(x + \alpha t) \\ s_2(x, y, t) &= C + \cos(y + \alpha t) - \alpha(\lambda + 1)\sin(y + \alpha t) \end{cases} \tag{4.12}$$

where C, α are constants and we take $C = 2, \alpha = 4$ in our tests. With the periodic boundary condition, the problem has an exact solution

$$\begin{aligned} u(x, y, t) &= C + \sin(x + \alpha t) + \sin(y + \alpha t), \\ Q_1(x, y, t) &= C - \alpha \sin(x + \alpha t), \\ Q_2(x, y, t) &= C - \alpha \sin(y + \alpha t). \end{aligned} \tag{4.13}$$

We compute to $T = 0.5$ with the time step $\tau = 0.1h, \tau = 0.02h, \tau = 0.01h$ for the $\mathcal{P}^2, \mathcal{P}^3, \mathcal{P}^4$ DG schemes, respectively, where $h = \min_{i,j}\{h_i^x, h_j^y\}$. The numerical solution without the positivity-preserving limiter is listed in Table 4.6 and the numerical solution with the positivity-preserving limiter is listed in Table 4.7. The last column $Nc(\%)$ in Table 4.7 is the proportion of the quadrature points modified by the positivity-preserving limiter. Although a few quadrature points have been modified by the limiter, the introduction of the positivity-preserving limiter still does not affect the original accuracy of our high-order entropy stable DG scheme.

4.2.3 Accuracy test: Nonlinear nonlocal electron heat transport model

Take the nonlinear nonlocal electron heat flux $k(u) = \frac{u^2}{2}, \lambda = 0.05$, we consider the initial value problem with two source terms $s_1(x, y, t), s_2(x, y, t)$,

$$\begin{cases} \frac{\partial u}{\partial t} &= -\frac{\partial Q_1}{\partial x} - \frac{\partial Q_2}{\partial y}, \quad (x, y) \in [0, 2\pi] \times [0, 2\pi] \\ Q_1 &= -u\frac{\partial u}{\partial x} + \lambda(\frac{\partial^2 Q_1}{\partial x^2} + \frac{\partial^2 Q_1}{\partial y^2}) + s_1 \\ Q_2 &= -u\frac{\partial u}{\partial y} + \lambda(\frac{\partial^2 Q_2}{\partial x^2} + \frac{\partial^2 Q_2}{\partial y^2}) + s_2 \\ u(x, y, 0) &= C + \sin(x) + \sin(y) \\ s_1(x, y, t) &= C - (\lambda + 1)e^{-t}\cos(x) + e^{-t}\cos(x)\left(C + e^{-t}(\sin(x) + \sin(y))\right) \\ s_2(x, y, t) &= C - (\lambda + 1)e^{-t}\cos(y) + e^{-t}\cos(y)\left(C + e^{-t}(\sin(x) + \sin(y))\right) \end{cases} \tag{4.14}$$

Table 4.6: Accuracy test: error and order of the two-dimensional linear nonlocal electron heat transport model with the alternative numerical flux (3.5) and without the positivity-preserving limiter.

	N_x, N_y	L_1 error	order	L_2 error	order	L_∞ error	order
$\mathcal{P}^2$	10	2.7036E-02		1.7579E-02		4.2379E-02	
	20	3.4217E-03	2.98	2.2286E-03	2.98	5.5419E-03	2.93
	40	4.2657E-04	3.00	2.7805E-04	3.00	6.9044E-04	3.00
	60	1.2618E-04	3.00	8.2270E-05	3.00	2.0460E-04	3.00
	80	5.3182E-05	3.00	3.4679E-05	3.00	8.6272E-05	3.00
	N_x, N_y	L_1 error	order	L_2 error	order	L_∞ error	order
$\mathcal{P}^3$	10	8.8328E-04		5.7913E-04		1.6119E-03	
	20	5.5060E-05	4.00	3.6086E-05	4.00	1.0061E-04	4.00
	40	3.4414E-06	4.00	2.2571E-06	4.00	6.3213E-06	3.99
	60	6.8312E-07	3.99	4.4837E-07	3.99	1.2588E-06	3.98
	80	2.1756E-07	3.98	1.4290E-07	3.97	4.0232E-07	3.97
	N_x, N_y	L_1 error	order	L_2 error	order	L_∞ error	order
$\mathcal{P}^4$	10	2.4025E-05		1.6249E-05		4.3370E-05	
	20	7.4950E-07	5.00	5.0483E-07	5.01	1.3553E-06	5.00
	40	2.4174E-08	4.95	1.6033E-08	4.98	4.0112E-08	5.08
	60	3.5409E-09	4.74	2.2860E-09	4.80	4.8003E-09	5.24

where C is a constant. With the periodic boundary condition, the problem has an exact solution

$$\begin{aligned} u(x,y,t) &= C + e^{-t}(\sin(x) + \sin(y)), \\ Q_1(x,y,t) &= C - e^{-t}\cos(x), \\ Q_2(x,y,t) &= C - e^{-t}\cos(y). \end{aligned} \tag{4.15}$$

We compute to $T = 0.5$ with the time step $\tau = 0.1h, \tau = 0.02h, \tau = 0.01h$ for the $\mathcal{P}^2, \mathcal{P}^3, \mathcal{P}^4$ DG schemes, respectively, where $h = \min_{i,j}\{h_i^x, h_j^y\}$. The numerical results are listed in Table 4.8.

Similar to the one-dimensional case, the two-dimensional high-order entropy stable and positivity-preserving DG scheme can also achieve optimal accuracy for all the models and it can also be extended to higher order with more quadrature points and higher-order SSP-RK time discretization method.

Table 4.7: Accuracy test: error and order of the two-dimensional linear nonlocal electron heat transport model with the alternative numerical flux (3.5) and the positivity-preserving limiter. Nc is the percentage of quadrature points modified by the positivity-preserving limiter.

	N_x, N_y	L_1 error	order	L_2 error	order	L_∞ error	order	$Nc(\%)$
$\mathcal{P}^2$	10	2.6859E-02		1.7520E-02		4.3998E-02		1.33E-01
	20	3.4268E-03	2.97	2.2351E-03	2.97	5.9392E-03	2.89	2.81E-02
	40	4.2713E-04	3.00	2.7862E-04	3.00	1.0488E-03	2.50	5.90E-03
	60	1.2645E-04	3.00	8.2562E-05	3.00	4.3331E-04	2.18	2.41E-03
	80	5.3254E-05	3.01	3.4758E-05	3.01	1.9226E-04	2.82	1.35E-03
	N_x, N_y	L_1 error	order	L_2 error	order	L_∞ error	order	$Nc(\%)$
$\mathcal{P}^3$	10	8.8857E-04		5.8090E-04		1.6125E-03		1.88E-02
	20	5.5096E-05	4.01	3.6093E-05	4.01	1.0062E-04	4.00	1.56E-03
	40	3.4420E-06	4.00	2.2573E-06	4.00	6.3237E-06	3.99	4.88E-04
	60	6.8311E-07	3.99	4.4838E-07	3.99	1.2594E-06	3.98	1.88E-04
	80	2.1755E-07	3.98	1.4291E-07	3.97	4.0248E-07	3.97	1.10E-04
	N_x, N_y	L_1 error	order	L_2 error	order	L_∞ error	order	$Nc(\%)$
$\mathcal{P}^4$	10	2.4034E-05		1.6251E-05		4.3368E-05		5.00E-04
	20	7.4950E-07	5.00	5.0483E-07	5.01	1.3553E-06	5.00	6.25E-05
	40	2.4174E-08	4.95	1.6033E-08	4.98	4.0115E-08	5.08	1.26E-05
	60	3.5406E-09	4.74	2.2858E-09	4.80	4.8034E-09	5.23	2.32E-06

Table 4.8: Accuracy test: error and order of the two-dimensional nonlinear nonlocal electron heat transport model with the alternative numerical flux (3.5).

	N_x, N_y	L_1 error	order	L_2 error	order	L_∞ error	order
$\mathcal{P}^2$	10	3.8994E-03		2.6740E-03		6.5606E-03	
	20	4.7009E-04	3.05	3.2260E-04	3.05	7.3493E-04	3.16
	40	5.8196E-05	3.01	3.9988E-05	3.01	8.7598E-05	3.07
	60	1.7286E-05	2.99	1.1849E-05	3.00	2.5511E-05	3.04
	80	7.3254E-06	2.98	5.0083E-06	2.99	1.0676E-05	3.03
	N_x, N_y	L_1 error	order	L_2 error	order	L_∞ error	order
$\mathcal{P}^3$	10	2.1230E-04		1.4721E-04		6.2032E-04	
	20	1.2943E-05	4.04	8.9046E-06	4.05	3.4220E-05	4.18
	40	8.0490E-07	4.01	5.5200E-07	4.01	1.9532E-06	4.13
	60	1.5924E-07	4.00	1.0912E-07	4.00	3.7239E-07	4.09
	80	5.0559E-08	3.99	3.4628E-08	3.99	1.1623E-07	4.05
	N_x, N_y	L_1 error	order	L_2 error	order	L_∞ error	order
$\mathcal{P}^4$	10	8.4578E-06		6.0710E-06		3.0277E-05	
	20	2.6838E-07	4.98	1.8614E-07	5.03	7.8894E-07	5.26
	40	8.5576E-09	4.97	5.8719E-09	4.99	2.3311E-08	5.08
	60	1.2187E-09	4.81	8.1762E-10	4.86	3.0180E-09	5.04

4.2.4 The positivity-preserving test

We construct a circular discontinuous function noted as the cylinder function in $[0,1]\times[0,1]$ and take $C(0.5, 0.5)$ as the center of the circle

$$u(x,y,0) = \begin{cases} 1 & d(x,y) \le r \\ 0 & d(x,y) > r \end{cases}, \quad d(x,y) = \sqrt{(x-0.5)^2 + (y-0.5)^2} \tag{4.16}$$

where we take $r = \frac{1}{4}$ in the numerical test. Take the cylinder function (4.16) as the initial function for our two-dimensional linear nonlocal electron heat transport model with $k(u) = u, \lambda = 2.5 \times 10^{-4}$.

Figure 4.10 is the projection of the three-dimensional image on the $x - y$ plane which shows the numerical solutions with the positivity-preserving limiter for the nonlocal model. In this problem, negative values of the quadrature points emerge at the first several time steps and they need to be modified by the positivity-preserving limiter which has been shown by the white symbols in the right subfigure of Figure 4.10.

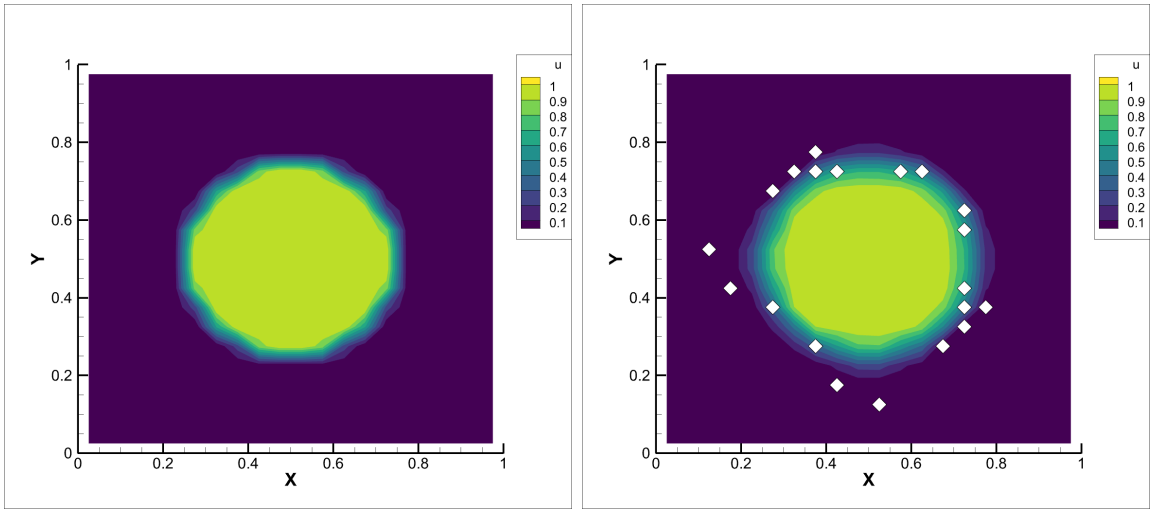

Figure 4.10: The numerical results for the two-dimensional DG scheme with $k(u) = u, \lambda = 2.5 \times 10^{-4}, \tau = \lambda$ for the test function (4.16) with the positivity-preserving limiter. Left: the initial cylinder function; Right: the numerical results at the first time step with the positivity-preserving limiter. The white symbols in the right profile represent the cells which have been modified by the positivity-preserving limiter.

4.2.5 Comparison between the local and nonlocal electron heat transport models

Take the following function

$$u(x,y,0) = \begin{cases} C & x+y < 0.5 \\ C + \sin(2\pi(x+y)+\pi) & 0.5 \le x+y < 1 \\ C + 0.1\sin(2\pi(x+y)) & 1 \le x+y < 1.5 \\ C & x+y \ge 1.5 \end{cases} \quad (x,y) \in [0,1]\times[0,1], \quad C = 0.5, \tag{4.17}$$

as the initial function for the two-dimensional nonlinear local and nonlocal electron heat transport models with $k(u) = \frac{u^2}{2}, \lambda = 0.01$. Similar to Section 4.1.5, we compare the temperature of the two models near the extrema $x + y = 1.25$. In Figure 4.11, we use different color surfaces to represent numerical solutions at the different time. We show the values at the quadrature points along $x = y$ in Figure 4.12 and these results are similar to the one-dimensional results in Figure 4.7 which can also explain the difference between these two models.

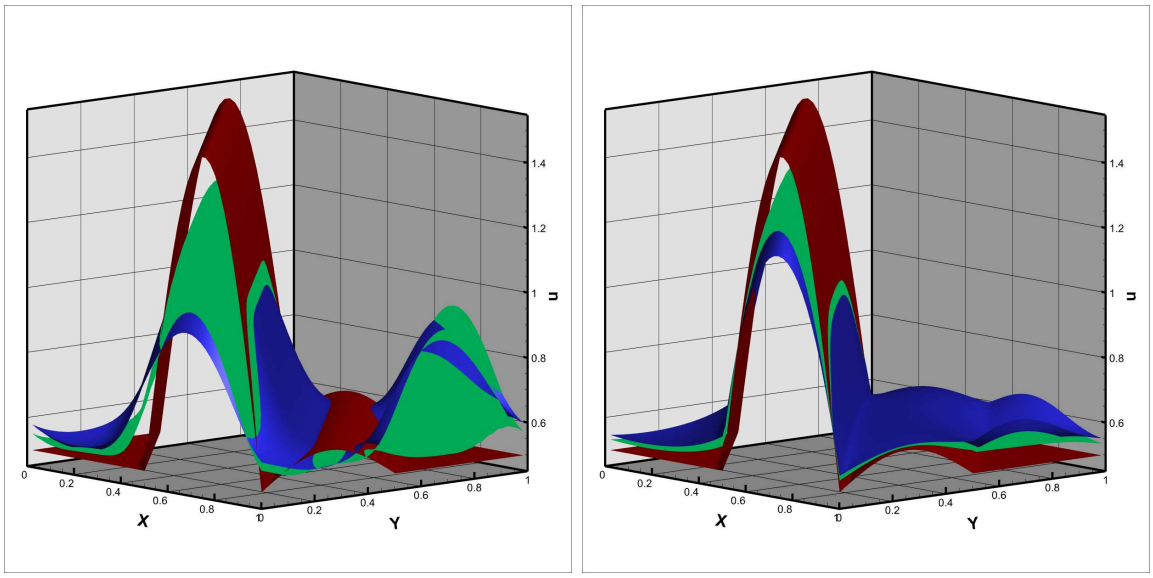

Figure 4.11: The two-dimensional local and nonlocal electron heat transport models at $t = 0.005$. Left: the local model; Right: the nonlocal model. Red surfaces, green surfaces and blue surfaces represent $t = 0$, $t = 0.0025$ and $t = 0.005$, respectively.

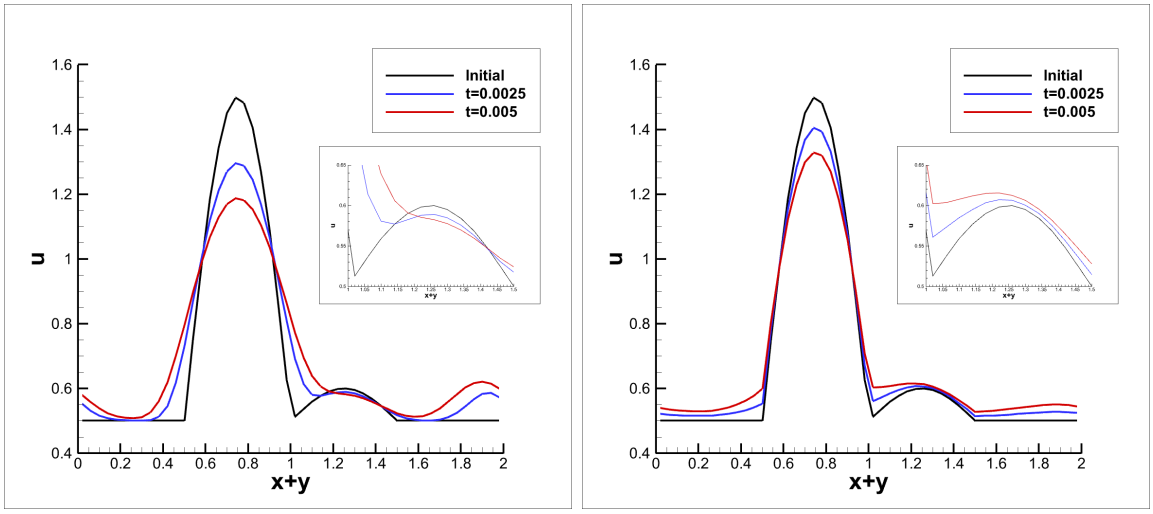

Figure 4.12: The two-dimensional local and nonlocal electron heat transport models at $t = 0.005$ with the values at the quadrature points along $x = y$. Left: the local model; Right: the nonlocal model.

5 Concluding remarks

In this paper, aiming at the nonlocal electron heat transport model, we develop a high-order entropy stable and positivity-preserving DG scheme in one and two dimensions with the SSP-RK time discretization and the scheme can achieve high-order accuracy both in space and time. By the scaling positivity-preserving limiter, our DG scheme can preserve positivity for temperature without destroying the original accuracy and the restrictions on the time step can almost be ignored which have been analyzed numerically. In the numerical experiments, we have verified the properties of high-order accuracy, entropy stability, and positivity-preserving of our scheme. Furthermore, we demonstrate several numerical tests to show the differences between the local and nonlocal electron heat transport models and observe similar qualitative conclusions as those given in the literature. Near large temperature gradients, compared with the classical local electron heat transport model, the nonlocal electron heat transport model has a wider range of influence but lower change on the temperature. Especially in Subsection 4.1.5 and Subsection 4.2.5, we observe counter-intuitive decay of temperature at the local extrema in the nonlocal model which exactly explains the flux reduction phenomenon in the electron heat transport model.

The high-order DG scheme for the nonlocal electron heat transport model, together with entropy stability and positivity-preserving property, can be extended to two-dimensional unstructured meshes and to three dimensions, which constitutes our future work. Besides that, we will attempt to apply our high-order, positivity-preserving, and entropy stable DG scheme in the simulation of laser-driven ICF by coupling with the other physical processes.

A Appendix: Stability property for the one-dimensional nonlocal electron heat transport model

Consider the one-dimensional nonlocal electron heat transport model (2.1) with $\lambda > 0$ in the linear case $k(u) = u$,

$$\begin{cases} \partial_t u = -\partial_x Q \\ Q = -\partial_x u + \lambda \partial_{xx} Q \\ u(x,0) = u_0(x), \quad x \in [0, 2\pi], \quad t > 0, \end{cases} \tag{A.1}$$

where the initial condition $u_0(x)$ is a 2π-periodic function. We take the Fourier transform with respect to the spatial variable x and the above model with a single mode initial condition becomes an ordinary differential equation,

$$\begin{cases} \partial_t \hat{u}(\omega,t) = -i\omega \hat{Q}(\omega,t) \\ \hat{Q}(\omega,t) = -i\omega \hat{u}(\omega,t) - \lambda\omega^2 \hat{Q}(\omega,t) \\ \hat{u}(\omega,0) = \hat{u}_0(\omega) \end{cases} \tag{A.2}$$

where $\hat{u}(\omega,t), \hat{Q}(\omega,t)$ are the Fourier transform of $u(x,t), Q(x,t)$, respectively, then we have

$$\begin{cases} \partial_t \hat{u}(\omega,t) = \frac{-\omega^2}{1+\lambda\omega^2} \hat{u}(\omega,t) \\ \hat{u}(\omega,t) = \hat{u}_0(\omega) \end{cases} \Rightarrow \hat{u}(\omega,t) = \hat{u}_0(\omega) e^{-\frac{\omega^2}{1+\lambda\omega^2} t}. \tag{A.3}$$

Thus, for the general L^2 initial condition $u_0(x) = \frac{1}{\sqrt{2\pi}} \sum_{\omega=-\infty}^{+\infty} e^{i\omega x} \hat{u}_0(\omega)$, we have

$$u(x,t) = \frac{1}{\sqrt{2\pi}} \sum_{\omega=-\infty}^{+\infty} e^{-\frac{\omega^2}{1+\lambda\omega^2} t} e^{i\omega x} \hat{u}_0(\omega).$$

Since $0 \le \frac{\omega^2}{1+\lambda\omega^2} \le \frac{1}{\lambda}$ for all ω, so we know the solution u is stable from Parseval's relation,

$$||u(\cdot,t)||^2 = \sum_{\omega=-\infty}^{+\infty} |e^{-\frac{\omega^2}{1+\lambda\omega^2} t} \hat{u}_0(\omega)|^2 \le ||u_0(\cdot)||^2.$$

Furthermore, this conclusion can also be extended to the multi-dimensional cases. For the truly global model with $\lambda > 0$, the Fourier analysis for the linear case explains the fact that our numerical scheme is stable as long as the time step is upper-bounded by a constant, independent of the spatial mesh sizes, see Section 2.4 and Section 3.4 for more details.

References

[1] B. Ayuso, J. A. Carrillo, and C.-W. Shu, Discontinuous Galerkin methods for the one-dimensional VlasovPoisson system, Kinetic and Related Models, 4 (2011), 955-989.

[2] B. Ayuso, J. A. Carrillo, and C.-W. Shu, Discontinuous Galerkin methods for the multi-dimensional VlasovPoisson problem, Mathematical Models and Methods in Applied Sciences, 22 (2012), 1250042.

[3] A. V. Brantov and V. Yu. Bychenkov, Nonlocal transport in hot plasma. Part i, Plasma Physics Reports, 39 (2013), 698-744.

[4] A. V. Brantov and V. Yu. Bychenkov, Nonlocal transport in hot plasma. Part ii, Plasma Physics Reports, 40 (2014), 505-563.

[5] T. Chen and C.-W. Shu, Entropy stable high-order discontinuous Galerkin methods with suitable quadrature rules for hyperbolic conservation laws, Journal of Computational Physics, 345 (2017), 427-461.

[6] T. Chen and C.-W. Shu, Review of entropy stable discontinuous Galerkin methods for systems of conservation laws on unstructured simplex meshes, CSIAM Transactions on Applied Mathematics, 1 (2020), 1-52.

[7] Y. Cheng and C.-W. Shu, A discontinuous Galerkin finite element method for time dependent partial differential equations with higher order derivatives, Mathematics of Computation, 77 (2008), 699-730.

[8] B. Cockburn, S. Hou, C.-W. Shu, The Runge-Kutta local projection discontinuous Galerkin finite element method for conservation laws II: the multidimensional case, Mathematics of Computation, 54 (1990), 545-581.

[9] B. Cockburn, S.-Y. Lin, C.-W. Shu, TVB Runge-Kutta local projection discontinuous Galerkin finite element method for conservation laws III: one dimensional systems, Journal of Computational Physics, 84 (1989), 90-113.

[10] B. Cockburn, C.-W. Shu, TVB Runge-Kutta local projection discontinuous Galerkin finite element method for conservation laws II: general framework, Mathematics of Computation, 52 (1989), 411-435.

[11] B. Cockburn, C.-W. Shu, The Runge-Kutta local projection P^1-discontinuous-Galerkin finite element method for scalar conservation laws, ESAIM: Mathematical Modeling and Numerical Analysis, 25 (1991), 337-361.

[12] B. Cockburn, C.-W. Shu, The RungeKutta discontinuous Galerkin method for conservation laws V: multidimensional systems, Journal of Computational Physics, 141 (1998), 199-224.

[13] B. Cockburn, C.-W. Shu, The local discontinuous Galerkin method for time-dependent convection-diffusion systems, SIAM Journal on Numerical Analysis, 35 (1998), 2440-2463.

[14] R. S. Cohen, L. Spitzer, and P. M. Routly, The electrical conductivity of an ionized gas, Physical Review, 80 (1950), 230-238.

[15] D. G. Colombant, W. M. Manheimer and M. Busquet, Test of models for electron transport in laser produced plasmas, Physics of Plasmas, 12 (2005), 072702.

[16] S. Gottlieb, C.-W. Shu and E. Tadmor, Strong stability-preserving high-order time discretization methods, SIAM Review, 43 (2001), 89-112.

[17] S. Hou, X.-D. Liu, Solutions of multi-dimensional hyperbolic systems of conservation laws by square entropy condition satisfying discontinuous Galerkin method, Journal of Scientific Computing, 31 (2007), 127-151.

[18] G. S. Jiang, C.-W. Shu, On a cell entropy inequality for discontinuous Galerkin methods, Mathematics of Computation, 62 (1994), 531-538.

[19] K. Li and W. Y. Huo, Nonlocal electron heat transport under the non-Maxwellian distribution function, Physics of Plasmas, 27 (2020), 062705.

[20] Y. Liu and C.-W. Shu, Error analysis of the semi-discrete local discontinuous Galerkin method for semiconductor device simulation models, Science China Mathematics, 53 (2010), 3255-3278.

[21] Y. Liu and C.-W. Shu, Analysis of the local discontinuous Galerkin method for the drift-diffusion model of semiconductor devices, Science China Mathematics, 59 (2016), 115-140.

[22] J. F. Luciani, P. Mora and J. Virmont, Nonlocal heat transport due to steep temperature gradients, Physical Review Letters, 51 (1983), 1664-1667.

[23] T. Qin and C.-W. Shu, Implicit positivity-preserving high-order discontinuous Galerkin methods for conservation laws, SIAM Journal on Scientific Computing, 40 (2018), A81-A107.

[24] G. P. Schurtz, Ph. D. Nicolaï and M. Busquet, A nonlocal electron conduction model for multidimensional radiation hydrodynamics codes, Physics of plasmas, 7 (2000), 4238-4249.

[25] L. Spitzer and R. Härm, Transport phenomena in a completely ionized gas, Physical Review, 89 (1953), 977-981.

[26] Z. Sun, J. A. Carrillo, and C.-W. Shu, A discontinuous Galerkin method for nonlinear parabolic equations and gradient flow problems with interaction potentials, Journal of Computational Physics, 352 (2018), 76-104.

[27] Z. Sun, J. A. Carrillo, and C.-W. Shu, An entropy stable high-order discontinuous Galerkin method for cross-diffusion gradient flow systems, Kinetic and Related Models, 12 (2019), 885-908.

[28] C. Wang, X. Zhang, C.-W. Shu and J. Ning, Robust high order discontinuous Galerkin schemes for two-dimensional gaseous detonations, Journal of Computational Physics, 231 (2012), 653-665.

[29] Y. Xing, X. Zhang and C.-W. Shu, Positivity-preserving high order well-balanced discontinuous Galerkin methods for the shallow water equations, Advances in Water Resources, 33 (2010), 1476-1493.

[30] X. Zhang, On positivity-preserving high order discontinuous Galerkin schemes for compressible Navier-Stokes equations, Journal of Computational Physics, 328 (2017), 301-343.

[31] X. Zhang, C.-W. Shu, On maximum-principle-satisfying high order schemes for scalar conservation laws, Journal of Computational Physics, 229 (2010), 3091-3120.

[32] X. Zhang, C.-W. Shu, On positivity preserving high order discontinuous Galerkin schemes for compressible Euler equations on rectangular meshes, Journal of Computational Physics, 229 (2010), 8918-8934.

[33] X. Zhang, C.-W. Shu, Maximum-principle-satisfying and positivity-preserving high-order schemes for conservation laws: survey and new developments, Proceedings of the Royal Society A, 467 (2011), 2752-2776.

[34] X. Zhang and C.-W. Shu, Positivity-preserving high order finite difference WENO schemes for compressible Euler equations, Journal of Computational Physics, 231 (2012), 2245-2258.

[35] Y. Zhang, X. Zhang and C.-W. Shu, Maximum-principle-satisfying second order discontinuous Galerkin schemes for convectiondiffusion equations on triangular meshes, Journal of Computational Physics, 234 (2013), 295-316.

[36] W. Zhang, H. Cai, B. Du, D. Kang, S. Zou and S. Zhu, Full particle-in-cell simulation of the formation and structure of a collisional plasma shock wave, Physical Review E, 103 (2021), 023213.